NASA/TM—2005-213457

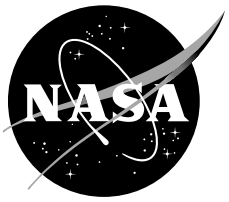

Apollo Capsule Optimization for Improved Stability and Computational/Experimental Data Comparisons

Susan E. Cliff
Ames Research Center, Moffett Field, California

Scott D. Thomas
Raytheon ITSS
Ames Research Center, Moffett Field, California

May 2005

The NASA STI Program Office . . . in Profile

Since its founding, NASA has been dedicated to the advancement of aeronautics and space science. The NASA Scientific and Technical Information (STI) Program Office plays a key part in helping NASA maintain this important role.

The NASA STI Program Office is operated by Langley Research Center, the Lead Center for NASA's scientific and technical information. The NASA STI Program Office provides access to the NASA STI Database, the largest collection of aeronautical and space science STI in the world. The Program Office is also NASA's institutional mechanism for disseminating the results of its research and development activities. These results are published by NASA in the NASA STI Report Series, which includes the following report types:

- TECHNICAL PUBLICATION. Reports of completed research or a major significant phase of research that present the results of NASA programs and include extensive data or theoretical analysis. Includes compilations of significant scientific and technical data and information deemed to be of continuing reference value. NASA's counterpart of peer-reviewed formal professional papers but has less stringent limitations on manuscript length and extent of graphic presentations.

- TECHNICAL MEMORANDUM. Scientific and technical findings that are preliminary or of specialized interest, e.g., quick release reports, working papers, and bibliographies that contain minimal annotation. Does not contain extensive analysis.

- CONTRACTOR REPORT. Scientific and technical findings by NASA-sponsored contractors and grantees.

- CONFERENCE PUBLICATION. Collected papers from scientific and technical conferences, symposia, seminars, or other meetings sponsored or cosponsored by NASA.

- SPECIAL PUBLICATION. Scientific, technical, or historical information from NASA programs, projects, and missions, often concerned with subjects having substantial public interest.

- TECHNICAL TRANSLATION. English-language translations of foreign scientific and technical material pertinent to NASA's mission.

Specialized services that complement the STI Program Office's diverse offerings include creating custom thesauri, building customized databases, organizing and publishing research results . . . even providing videos.

For more information about the NASA STI Program Office, see the following:

- Access the NASA STI Program Home Page at *http://www.sti.nasa.gov*

- E-mail your question via the Internet to help@sti.nasa.gov

- Fax your question to the NASA Access Help Desk at (301) 621-0134

- Telephone the NASA Access Help Desk at (301) 621-0390

- Write to:
  NASA Access Help Desk
  NASA Center for AeroSpace Information
  7121 Standard Drive
  Hanover, MD 21076-1320

NASA/TM—2005-213457

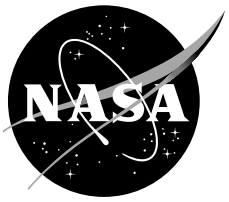

Apollo Capsule Optimization for Improved Stability and Computational/Experimental Data Comparisons

Susan E. Cliff
Ames Research Center, Moffett Field, California

Scott D. Thomas
Raytheon ITSS
Ames Research Center, Moffett Field, California

National Aeronautics and
Space Administration

Ames Research Center
Moffett Field, California 94035-1000

May 2005

Acknowledgments

The authors would like to thank Scott L. Lawrence for his efforts in obtaining all of the Navier–Stokes computations presented in this report, and his help in obtaining and evaluating several Apollo Project reports.

Available from:

NASA Center for AeroSpace Information
7121 Standard Drive
Hanover, MD 21076-1320
(301) 621-0390

National Technical Information Service
5285 Port Royal Road
Springfield, VA 22161
(703) 487-4650

CONTENTS

APOLLO CAPSULE OPTIMIZATION FOR IMPROVED STABILITY AND COMPUTATIONAL/EXPERIMENTAL DATA COMPARISONS

Susan E. Cliff and Scott D. Thomas

Ames Research Center

SUMMARY

Numerical optimization was employed on the Apollo Command Module to modify its external shape. The Apollo Command Module (CM) that was used on all NASA human spaceflights during the Apollo Space Program is stable and trimmed in an apex-forward (alpha of approximately 40 to 80 degrees) position. This poses a safety risk if the CM separates from the launch tower during abort. Optimization was employed on the Apollo CM to remedy the undesirable stability characteristics of the configuration. Geometric shape changes were limited to axisymmetric modifications that altered the radius of the apex (R_A), base radius (R_O), corner radius (R_C), and the cone half angle (θ), while the maximum diameter of the CM was held constant. The results of multipoint optimization on the CM indicated that the cross-range performance can be improved while maintaining robust apex-aft stability with a single trim point. Navier–Stokes computations were performed on the baseline and optimized configurations and confirmed the Euler-based optimization results. Euler analysis of ten alternative CM vehicles with different values of the above four parameters are compared with the published experimental results of numerous wind tunnel tests during the late 1960s. These comparisons cover a wide Mach number range and a full 180-degree pitch range and show that the Euler methods are capable of fairly accurate force and moment computations and can separate the vehicle characteristics of these ten alternative configurations.

INTRODUCTION

An unstructured Euler method has undergone extensive validation with experimental data on numerous space vehicles with blunt-based aft bodies. The validation is over subsonic to hypersonic Mach numbers and includes high angles of attack. The accuracy of the method is well understood, and the method is superior to preliminary design methods in the subsonic to low supersonic Mach number range. (The data and geometries are proprietary). This Euler method is coupled to a constrained gradient-based optimization algorithm and is used for aerodynamic shape optimization (ASO). Performance increments/improvements over baseline configurations held through wind tunnel tests and Navier–Stokes comparisons on a previous crew transfer vehicle (CTV) design. The method has been successfully used for multipoint complete configuration optimization with performance and stability/trim objectives on Lockheed Martin CTV configurations.

With the recent NASA mandate for the development of a manned crew exploration vehicle and the likely change from winged configurations to capsule designs, the Euler solver used in the optimization package was evaluated by comparison with the extensive wind tunnel data obtained during the Apollo Space Program. During this investigation the baseline Apollo CM (employed on all flights) was found to have an undesirable characteristic in that it is both stable and trimmed in an apex-forward position that poses a safety risk if the CM separates from the launch tower during abort. The Euler-based optimization program that was used successfully on winged configurations seemed ideally suited to perform optimization of the CM to remedy this undesirable characteristic. Alterations and additional components that were developed to eliminate the dual trim point of the Apollo capsule were built during the Apollo program, and the aerodynamic quantities of these vehicles were obtained through extensive wind tunnel tests. Computational fluid dynamics (CFD) codes have proliferated since the late 1960s and have become the testbeds for aerodynamic-based design changes with typically only limited wind tunnel testing. The wealth of test data from the 1960s remains significant to the calibration of CFD methods and was therefore used to compare with the Euler code on a series of 10 parametric designs of the capsule with shape changes that altered the radius of the apex (R_A), base radius (R_O), corner radius (R_C), and the cone half angle (θ), while holding the maximum diameter of the CM constant. Figure 1 depicts the variables used to change the capsule shape.

The four design parameters used were employed as design variables in a multipoint design optimization problem to eliminate the apex-forward trim point and improve the performance of the vehicle. Since the number of design variables was sufficiently small, a parametric study was also performed to find sets of parameters that were close to the optimum. This parametrically determined optimum is compared with the optimum found through the gradient-based optimization method.

The set of ten capsules (table 1) with experimental data are compared with the Euler solver at Mach numbers of 0.4, 0.7, 1.2, 1.65, 3.26, 3.27, and 5.0.

PARAMETRIC STUDY AND RESULTS

To properly assess an optimization of the Apollo capsule, a parametric study of the four design variables was initiated during the optimization of the Apollo capsule. The small number of geometric variables made a parametric study feasible. Each of the four design variables was altered over a range of reasonable values in equal increments to five different values and at three different angles of attack, requiring a total of 1875 (3×5^4) flow solutions. The values of the variables are provided below:

θ (degrees)	=	25.0	30.0	35.0	40.0	45.0
R_A (inches)	=	5.0	10.0	15.0	20.0	25.0
R_C (inches)	=	0.0	7.5	15.0	22.5	30.0
R_O (inches)	=	125.0	193.75	262.5	331.25	400.0

The capsule was assessed at Mach 3.26 and three angles of attack α = 75.0, 130.0, and 143.0 degrees, representing design points 1, 2, and 3, respectively. This large volume of data was evaluated

by applying the objective function used in the optimization problem to lift, drag, and moment coefficient data from these runs. The reference area of the semispan model used in the computations is 9313.2514 $in.^2$, the center of gravity (c.g.) was located at an axial location of 105.49 inches and a vertical location of –9.086 inches from the apex, and the average chord was 154 inches. This objective function comprises weighted terms involving forces and moment coefficient data from the three design points, as follows:

$$\text{Objective} = \sigma 1\,(CM_1 - 0.002)^2 + \sigma 2\,|CD_2/CL_2| + \sigma 3\,(CM_3)^2$$

The subscripts on the force and moment terms represent the design point of the solution. The variables $\sigma 1$, $\sigma 2$, and $\sigma 3$ were derived by finding the maximum value of each of the three terms in the parametric study, and scaling them such that:

$$\sigma 1 = 0.50 / \max\,[(CM_1 - 0.002)^2]$$
$$\sigma 2 = 0.25 / \max\,[|CD_2 / CL_2|]$$
$$\sigma 3 = 0.25 / \max\,[(CM_3 - 0.0)^2]$$

This weights the first term, forcing a positive pitching moment of 0.002 at $\alpha = 75$ degrees—to eliminate the trim point that occurs near this design point—as 50% of the objective function, with the other terms both weighted to 25% of the objective function.

The actual values of weighting terms determined from the parametric study are:

$\sigma 1 = 9.36754242347172$
$\sigma 2 = 0.0424317664785264$
$\sigma 3 = 15.5260032173313$

These weighting terms were then used in optimization. The starting objective function is set equal to 1.0 by the choice of the weighting terms described previously. Thus, the resulting weighted sum is expected to be of order 1 during optimization.

The parametric data can be visualized by multiplying the objective function at each of the 625 points of the four-dimensional matrix by 1000 and rounding its value to the nearest integer, as shown in table 2.

The data are shown as inner and outer matrix values where the outer matrix is for the half angle of the cone, θ, and apex radius, R_A, and the inner matrix is for the corner radius (columns for R_C of 0.0, 7.5, 15.0, 22.5, and 30.0 inches plotted left to right, respectively) and the base radius (rows for R_O of 125.0, 193.75, 262.5, 331.25, and 400.0 inches plotted from top to bottom, respectively). Since the objective function is to be minimized, the smaller integers represent better solutions. The lowest value of objective function using these σ values is 49 (colored red in table 2) and appears at position (4, 5, 1, 4); that is, outer matrix position of column 4, row 5, and inner matrix position of column 1, row 4, where $\theta = 40$, $R_A = 25$, $R_C = 0.0$, and $R_O = 331.25$. This will be called the best parametric shape. The objective function value was about 0.04948 for this combination of design variables.

Note that the optimum occurs where R_C is zero (the corner between the cone and the base is sharp). This may not be desirable in a practical design problem for aerodynamic heating concerns. If the zero-radius solutions are not feasible there are several choices with objective function values of 58 with larger R_C values of 7.5 degrees. The design space can be readily viewed by assigning colors to the original values of the four-dimensional matrix (figure 2). The color assignment is based on the values of the objective function, rather than the values in table 2. Slight differences in value are seen in the colors for equivalent values shown in the table. For example, the positions for $\theta = 35$ degrees, $R_A = 25$ inches, $R_C = 7.5$ inches (row 2 of inner matrix), and $R_O = 262.5$, 331.25, and 400 inches (columns 3–5) have values of 58. But these objective function values are actually 0.58108, 0.57557, and 0.57553, respectively, so there are slightly different shades of cyan in the colored graphic of figure 2. The baseline Apollo capsule C01 has values of $\theta = 33$ degrees, $R_A = 15.4$ inches, $R_C = 7.7$ inches, and $R_O = 184.8$ inches with a base width of 154.0 inches. The closest parametric 4-tuple for this would correspond to $\theta = 35$ degrees, $R_A = 15$ inches, $R_C = 7.5$ inches, and $R_O = 193.73$ inches at position (3, 3, 2, 2), which corresponds to a value of 65 in the table.

OPTIMIZATION DESCRIPTION

An Euler unstructured-tetrahedral-grid-based CFD code, AIRPLANE (ref. 1), is coupled to a constrained gradient-based optimization algorithm, NPSOL (ref. 2), to provide an aerodynamic shape optimization technique for the Systems Analysis & Integration Branch at NASA Ames Research Center. NPSOL is a constrained quasi-Newton finite-difference optimization method. Several codes were developed to facilitate aerodynamic shape optimization. These include adding multigrid capability to AIRPLANE, developing surface grid perturbation methods, developing a variety of mesh movement techniques, and the parallelization of these methods. In this capsule design case, the surface grids were developed by a new process, described in the next paragraph, and the multigrid option in the flow solver was not used.

A four-tuple (θ, R_A, R_C, R_O) determines a generating curve $y(x)$ in the symmetry plane, which then defines the capsule by rotation about the x axis. The capsule surface is made of a spherical apex, conical body, toroidal corner, and spherical base, with tangency at the connecting circles unless R_C is zero. Surface mesh generation is done by application of a special program named MKACM that creates strips of triangles from the waist (maximum diameter of the capsule), where $y(x) = 77$, marching to each axial extremity, driven by a maximum edge length requirement and a preference for equilateral triangles. For example, the baseline C01 surface mesh from minimum $x = 12.88$ to maximum $x = 142.7$ is defined by 9145 points, 18034 triangles, and 27178 edges, for which the average edge length is 1.85 inches with a standard deviation of 0.064. The whole surface mesh is shown in figure 3. Details of the apex, apex cone, cone corner base, and the corner base are shown in figures 4, 5, 6, and 7, respectively. The resulting surface mesh meets the Delaunay criterion, which is that the sphere balanced on each triangle contains no other mesh points than its vertices.

The optimization code has been successfully used in the recent past for the High-Performance Computing and Communication Program (HPCCP) by applying the method to the Ames Sharp CTV configurations. The resulting configurations were used for the approach and landing simulation database for the Virtual Flight Rapid Integration Test Environment (VF-RITE) project (ref. 3). These

methods more recently were used for the design of orbital space plane vehicles under a contract with Lockheed Martin Corporation, where improved stability characteristics and performance at multiple design points were attained.

Aerodynamic shape optimization is particularly amenable to unstructured-grid methods. Complete configuration multipoint numerical optimization can often begin within a few days for an unstructured method with the rapid generation of surface (triangles) and volume (tetrahedral) meshes of an unstructured method. A gradient approach was chosen since this tool is well suited for detailed aerodynamic design (the vehicle conceptual design was performed a priori). A gradient-based algorithm should require fewer function evaluations to find local minima or design improvements in contrast to non-gradient methods such as genetic algorithm techniques that are capable of finding the global minimum. However, the gradients calculated via finite differences are computationally expensive since they require at least two flow solutions for each design variable. Thus, a limited number of design variables is recommended to reduce the CPU time with the present method.

The AIRPLANE optimization process requires the user to supply a range of values for each design variable to limit the perturbations to those that are acceptable to the designer. The variable bounds are never exceeded since NPSOL is a constrained optimization method. The choice of variable bounds should be carefully considered before optimization begins. The ranges should be narrow enough to eliminate undesirable results, yet wide enough so that significant performance changes can be obtained by the optimizer. As the optimizer runs, it checks for stored solutions that may have already been computed, matching flow conditions and design variables. This is used to "restart" the optimization process because finding flow solutions is relatively time consuming—NPSOL itself executes very rapidly. If no existing solution is found, the code proceeds to create the surfaces of the vehicle, either through a body-of-revolution meshing method for capsule designs or through modification of the surfaces of the configurations using APSHAPER and APSHBODY (ref. 4). APSHAPER perturbs the triangulated surfaces of wing-type components, ensuring that the number of points and connectivity remain unchanged. It is capable of wing planform changes and dihedral in addition to wing sectional changes such as camber, thickness, and leading- and trailing-edge droop. It can also provide flap deflections as either true rotations or by shearing the wing for either leading- or trailing-edge flaps. APSHBODY is used to perturb "body-type" components. Perturbation on the fuselage can be applied vertically, spanwise, or radially. Fuselage camber and droop applied to either the fore or aft portion is also attainable.

When the surface mesh is established, the AIRPLANE volume mesh of tetrahedra is either deformed or regenerated. MESHMV (ref. 4), the mesh deformation package, preserves the number of points and connectivity of the original mesh and runs quickly. If this method inverts any tetrahedron, the whole mesh is automatically regenerated from scratch using MESH3D (ref. 5). In this capsule design effort, MESH3D was used to regenerate the volume meshes each time because the surface mesh generation program was allowed to change the number of surface points. Following this, AIRPLANE is run, and the aerodynamic lift coefficient (CL), drag coefficient (CD), and pitching moment coefficient (CM) are returned to NPSOL in order to compute the objective function.

APOLLO CAPSULE AERODYNAMIC CHARACTERISTICS

The Apollo capsule is known as the C01 configuration to distinguish it from the other nine capsules that were wind tunnel tested during the Apollo Program (table 1). The C01 configuration has these properties: $\theta = 33.0$ degrees, $R_A = 15.4$ inches, $R_C = 7.7$ inches, and $R_O = 184.8$ inches, with a base width of 154.0 inches. This capsule was used as the baseline configuration for optimization.

The baseline configuration lift, drag, and pitching moment coefficient characteristics were obtained for Mach 3.27 using the unstructured Euler code, AIRPLANE, in figures 8, 9, and 10. An angle of attack of zero degrees represents the apex-forward position, and thus 180 degrees angle of attack will position the vehicle with the base (or heat shield) forward. The ability of the Euler computational methods to predict the flow characteristics of this vehicle is very good for these flight conditions. These computational tools were not developed during the Apollo Program, hence wind tunnels were used extensively to obtain aerodynamic data bases for the Apollo configurations. The pitching moment coefficient data shows the design flaw of the Apollo configuration (figure 10). The multiple trim points are shown in both the experimental and computational data. The trim points that occur at pitch angles between about 50 and 85 degrees are undesirable because the apex is still forward and the vehicle is not protected by the blunt base that acts as a heat shield. In addition, the negative slope of the moment curve indicates that the vehicle can achieve stable trim, that is, the capsule will return to the trim point if perturbed from this position. This was a well-known problem of the isolated capsule during the Apollo Program. The remedy to ensure that the capsule heat shield would be in a forward attitude was to include deployable canard surfaces near the rocket nose of the launch escape vehicle (LEV) (ref. 6) and to allow the entire LEV to remain attached during an abort scenario. The LEV consists of the command module, tower assembly, and rocket body. The deployed canard surfaces cause the complete LEV to rotate so that the heat shield is forward. The canard surfaces also help to dampen the aerodynamic forces after the rotation maneuver.

OPTIMIZATION DISCUSSION AND RESULTS

The objective function and range of design variables were chosen to address the performance and (static stability) pitching moment characteristics of the capsule. Other system requirements are not addressed, such as the dynamic stability of the isolated capsule or the aerodynamic heat loads of the capsule. This optimization problem was set up to demonstrate the applicability of unstructured optimization to space capsule design, primarily as proof of concept to show that it is quite capable of achieving improved capsule designs for the currently mandated crew exploration vehicle. The objective function for optimization was described in detail in the parametric study section of this report. The optimization was a three-point design problem with each of the three design points at Mach 3.26. The three points were for three angles of attack, where the first term of the objective function was designed to modify the pitching moment at alpha of 75 degrees to a value of 0.002 to remove the trim point at this condition. The second term was to improve L/D (minimize D/L) at 130 degrees, and the third term was to maintain the trim point at alpha 143 degrees. These three terms are added together with weighting factors of 0.5, 0.25, and 0.25 for the three design points, respectively, to form a single objective function value that is to be minimized during optimization. The

angle of attack of 130 degrees was chosen because $(L/D)_{max}$ is obtained at this angle in the experimental data (ref. 7). The angle of attack of 143 degrees is the angle where trim occurred for the computational results from AIRPLANE.

The ranges of the design variables were chosen to be the same as those used for the parametric study, namely: $25 \le \theta \le 45$ degrees, $5 \le R_A \le 25$ inches, $0 \le R_C \le 30$ inches, and $125 \le R_O \le 400$ inches. NPSOL will not allow violation of these design variable constraints. In a true multidisciplinary design, each of the many disciplines would have inputs into the range of feasible values that these design variables could take on. Starting from the baseline C01 shape $(\theta, R_A, R_C, R_O) = (33, 15.4, 7.7, 184.8)$, an optimized solution was found at approximately (35.6, 14.17, 0.0, 297.8) with an objective function value of about 0.04954, which is within about 0.1% of the value found parametrically. The four defining parameters for the baseline C01 and subsequently designed Apollo Command Modules are listed together in table 3 for easy reference. Symmetry plane profiles of all members of the four-parameter family considered in this report are plotted in figure 11. The nominal center of gravity at $x = 105.49, y = -9.086,$ which was used to compute the pitching moment, is shown in each of the 14 profiles.

This first optimization required only 43 objective function evaluations (129 flow solutions), which is 7% of what was spent on the parametric study. NPSOL finds an acceptably small objective function by repeated application of gradient approximation and line search steps. Typically only two or three points are needed to approximate each partial derivative numerically, with the central point shared for each dimension. In the present case, it takes five function evaluations to get the first gradient. A suggested difference interval size to use for the first gradient, the expected function precision, a line search tolerance, and an optimality tolerance are parameters set by the operator, among many others. For this case, the values chosen were 1e-1, 1e-5, 1e-3, and 1e-4, respectively. Definitions of these control parameters are provided in the NPSOL documentation and are beyond the present scope to describe.

Surface pressure coefficient plots for the baseline C01 are shown in figures 12, 13, and 14 at the three design-point angles of attack, 75, 130, and 143 degrees, respectively, and at the base-forward trim angle, 143 degrees, in figure 15. The first three figures are flat shaded, while the fourth figure is shaded with two lights in order to cue the viewer's depth perception. Compare these with surface pressure coefficient plots in figures 16, 17, 18, and 19, for the best parametric shape. Here, the cone appears flatter and the corner is sharp, while the maximum diameter is preserved, and the base-forward trim angle is 139 degrees. Similar plots for the first parametric design are shown in figures 20, 21, 22, and 23. This shape is not as flat, but the corner is still sharp and the trim angle is also 139 degrees.

To evaluate the efficacy of an optimization run, consider the values of the objective function, the three terms that compose its sum (figure 24), and the values of the four design parameters at each evaluation (figures 25, 26, 27, and 28). In these five plots, the numbering starts at function evaluation number 0, which corresponds to the baseline C01 Apollo Command Module shape. The final evaluation is number 42, for a total of 43 evaluations. The optimal solution reported by NPSOL usually is not the last one evaluated, nor is it necessarily the smallest one ever found. The optimal solution should have an objective function that is within the set tolerance. In the present case, NPSOL reported that it could not meet the requested accuracy, but it selected as optimal the point at

evaluation number 33, which also happened to have the smallest objective. The initial objective function was 0.066202, the last value was 0.050072, and the optimal value reported by NPSOL was 0.049537 at evaluation number 33. The objective function is the sum of three terms. The performance term, involving the minimization of CD/CL at the second design point, $\alpha = 130$ degrees, dominated the objective function during the whole optimization run, even though the three sigma values were designed to weigh the terms in proportions 50:25:25. The reason for this is that the sigma values were determined by considering 625 points across the whole parametric space, but the optimizer did not have to go to every extreme. Given another opportunity, one might weigh the terms differently, but the present weights still validate the approach.

In this optimization run, the cone half angle, θ, and the apex radius, R_A, stayed well within their bounds (figures 25 and 26, respectively). On the other hand, the corner radius, R_C, dropped to zero right away and stayed there, for the most part (figure 27). The fourth design parameter, the base radius, R_O, hit the upper limit at 400 only one time during a search (figure 28) at evaluation number 27—the objective function spiked there, too, but NPSOL recovered, as expected.

Both the best parametric and NPSOL optimization approaches resulted in a sharp corner, $R_C = 0$, which was permitted by the limits imposed. Pitching moment curves for the baseline C01, best parametric shape, and this first optimized shape are shown in figure 29. A stable trim point is predicted near $\alpha = 65$ degrees for C01. The value of CM for the latter two shapes remains positive near the original apex-forward stable trim point, as desired. The CM curve for the best parametric case at (40, 25, 0, 331.25) plots above the optimized case CM in this region, indicating that NPSOL found a shape with a smaller pitching moment penalty at the first design point. Trim at the third design point was not achieved at $\alpha = 143$ degrees, but it is an acceptable trade-off. Both the best parametric shape and the optimized shape have stable base-forward trim points at about $\alpha = 139$ degrees.

Figure 29 also shows Navier–Stokes predictions for the optimized shape (refs. 8–9) that are in good agreement with the pitching moments predicted by the Euler flow solver, at $\alpha = 60$, 90, 120, and 150 degrees. Three more Navier–Stokes comparisons, at $\alpha = 0$, 30, and 180 degrees, are shown in figure 30.

Lift-to-drag performance curves are plotted in figure 31 for baseline C01 and the two designs over pitch angles 60 to 150 degrees. The objective function is designed to maximize L/D at the second design point, $\alpha = 130$ degrees. Both of the new designs have higher L/D at the second design point, and the angle for which maximum L/D occurs is lower in each case. L/D for the optimized shape is lower at $\alpha = 130$ degrees than the value for the best parametric shape, which is another acceptable trade-off. To complete the comparison, figure 32 shows performance curves between pitch angles 0 to 180 degrees.

A second optimization was run subsequently, starting from the same initial baseline and with the same scaling, but changing the objective function so that CM larger than 0.002 added nothing to the objective function at the first design point, where $\alpha = 75$ degrees. The extra freedom resulted in an optimized shape at parameter values of approximately (44.99, 14.18, 0.0, 385.4) with an objective function of about 0.04197, which is 15% lower than what was found parametrically. In this case, the cone half angle θ bounced against the specified upper limit of 45 degrees, and the corner $R_C = 0$ turned out sharp again. The pitching moment near $\alpha = 75$ degrees turned out more positive than be-

fore because there was no penalty for going over the target CM. Compare surface pressure coefficient plots in figures 33, 34, 35, and 36, for the second optimized design, with earlier pressure coefficient figures. This optimization required 58 objective function evaluations. The objective function history is plotted for the second optimization in figure 37. The initial objective function was 0.066202, the last value was 0.042130, and the optimal value reported by NPSOL was 0.041970 at evaluation number 23. The lowest objective function was number 40 with a value of 0.041684. Observe that in the fourth gradient NPSOL used three-point numerical approximations to the partial derivatives. The pitching moment penalty at the first design point went to zero right away because of the way it was designed. The histories of design parameters are plotted in figures 38, 39, 40, and 41.

A third optimization was run that combined the objective function just described with a lower limit on the corner radius, $R_C = 5$ inches. In this case the optimized solution shape was (45, 16, 5, 400) with an objective function value of 0.04463. Compare the shapes and surface pressures in figures 42–45 with figures 20–23 and 33–36. Only the apex radius, $R_A = 16$, did not hit a range limit. The goal of eliminating the apex-forward stable trim condition was again achieved, and the optimization finished in 57 evaluations. The objective function history is plotted for the third optimization in figure 46, and the histories of design parameters are plotted in figures 47, 48, 49, and 50. The initial objective function was 0.066202, the last value was 0.044671, and the optimal value reported by NPSOL was 0.044634 at evaluation number 55, which was also the lowest objective function. For gradients, NPSOL used only two-point numerical approximations to the partial derivatives. The moment penalty at the first design point (term 1) went to zero right away because of the way it was designed. The performance term at the second design point dominated the objective function. The trim term at the third design point stayed under control, near zero, the whole time.

Pitching moment curves for the baseline C01 and the three NPSOL optimized shapes are shown in figure 51. The first optimization penalized shapes for which CM exceeded 0.002, but the other two optimizations penalized only shapes with CM lower than 0.002, so CM at $\alpha = 75$ for the first case is the lowest of the three optimized shapes. The CM curve generally shifts up, in the order of optimizations 1, 2, and 3, and the third optimization turns out with base-forward stable trim closer to the baseline than the other two. It may be coincidence that only the baseline and the third optimizations have round corners.

Lift-to-drag performance curves are plotted in figure 52 for the baseline C01 and the three NPSOL optimized shapes. All three optimized shapes perform better at design point 2 than the baseline (where $\alpha = 130$ degrees).

COMPUTATIONAL DATA CORROBORATION OF OPTIMIZED CAPSULE EULER / EXPERIMENTAL DATA CORROBORATION

Euler computations were performed on 10 capsules with the parameters shown in table 1. These 10 full-scale test models were wind tunnel tested in a large number of test facilities. All of the wind tunnel data presented were taken from reference 7 and are for static tests that were conducted using

sting mounted models attached to strain-gauge balances to measure the force and moment coefficient data. The reader is referred to reference 7 for further detail on the test and accuracy of the data.

AIRPLANE computations were performed for the 10 configurations at Mach numbers of 1.65, 3.26, 3.27, and 5.0. Additional computations were obtained at Mach 0.4, 0.7, and 1.2 for the C01 configuration. The computational angles of attack ranged from 0 to 180 degrees with 5-degree increments. The pitching moment coefficients of the wind tunnel data and computational predictions are compared for all configurations at Mach 1.65, 3.26 (3.27 for C01), and 5.0. The wind tunnel data were obtained by hand digitizing the data from an electronically scanned version of reference 7. The data at Mach 1.65 are shown in figure 53. Most of the experimental data were taken only for $120 \leq \alpha \leq 180$, whereas the AIRPLANE computations were from 0 to 180 degrees. The data and computations over the entire range of angles of attack are shown in figure 54. The data and computation comparisons for angles of attack of 120 to 180 degrees are shown in figure 55. Here, in figure 55, lies the evidence that the Euler methods are capable of predicting the differences in moment coefficient data between geometrically similar objects. Referring back to table 1, we see that C08, C02, C09, and C10 have cone angles $\theta = 30$, 33, 36, and 40 degrees, respectively. Considering respective pairs, they differ in cone angle by 3, 3, and 4 degrees. The increments between the experimental data compare well with the increments between the computational predictions. The actual values of the pitching moment also compare fairly well. Configurations C01 and C02 differ in the apex radius, $R_A = 15.4$ and 9.152, respectively. Reducing the apex radius by approximately 6 inches has little effect on the pitching moment characteristics. The computational data show the same result. However, the actual values of the CM predictions differ slightly more than for the C08-C02-C09-C10 data. C03, C02, C04, and C05 differ by corner radius, $R_C = 0$, 7.7, 15.4, and 23.1 inches, respectively (equal steps), and the increments between the test data are well predicted by the computations. Here again the actual value is shifted slightly, but the increments are well predicted. C06, C02, and C07 represent base radius changes, $R_O = 154$, 184.8, and 215.6, respectively (equal steps). The increments are also very well predicted by the Euler computations.

Data and computation comparisons for Mach 3.26 for C02–C10 and Mach 3.27 for C01 are shown in figures 56, 57, and 58. The increments are well captured overall by the Euler computational predictions. Inviscid solutions almost invariably predict more negative (nose down) pitching moments than viscous (real world) results, though the differences are small. The overall characteristics of the moment curves are quite similar for Mach 1.65 and 3.26; compare figures 55 and 58.

Data and computation comparisons for Mach 5.0 are shown in figures 59, 60, and 61. The computational predictions compare with experiment in absolute value better for configurations C04, C05, and C08 than was seen for the lower Mach number results, but poorer correlations are seen for C09 and C10 configurations. Compare figures 55, 58, and 61 (Mach 1.65, 3.26, and 5, respectively). Looking solely at the incremental differences between the models, the computational predictions continue to be able to "see" the differences in the configurations at Mach 5.0. Mach 5.0 is about the upper Mach number limit of the Euler computational method. The strong shocks from larger hypersonic Mach numbers would require increased dissipation in the flow solver to achieve convergence, and this would invalidate higher Mach number solutions.

The C01 configuration computations are also compared to the experimental data at lower Mach numbers. The lift and drag comparisons are shown for Mach 1.65 and 5.0 in figures 62, 63, 64, and

65. Mach 3.27 lift and drag results were shown previously in figures 8 and 9. The experimental data for the C01 includes the lower angles of attack and comparisons are over the full 180-degree range. The lift coefficient correlations are very good at Mach 1.65 (figure 62). There is some uncertainty in the lower angle-of-attack data in the experimental data, shown by the multivalued data points. The drag coefficient correlations are poorer than the lift comparisons (figure 63). The Mach 5.0 lift and drag coefficient correlations between experiment and the Euler computations are quite good (figures 64 and 65). The correlations improve with increasing Mach number.

The subsonic, transonic, and low supersonic Mach number pitching moment coefficient data for the C01 configuration are shown in figures 66, 67, and 68. The moment coefficient data from experiment was digitized and compared with the Euler computations. Figure 66 compares the Mach 0.4 results. Very poor correlation is obtained. The computations are unable to predict zero lift and hence zero moment for the symmetrical configurations at angles of attack of 0, 90, and 180 degrees. Flow around a blunt-bodied object is likely to be unsteady. The steady-state solutions obtained with the computations are clearly unable to accurately predict the flow characteristics.

CONCLUDING REMARKS

A new automated surface mesh generation method was developed for application to parametrically defined capsule shapes. This method proved to be robust and produced high-quality surface meshes. This method extends the existing set of design variables, which are capable of nearly complete configuration design changes to include those applicable to capsule design.

Multipoint optimization was performed on the Apollo Command Module to modify the exterior shape by altering the four vehicle-defining design variables. The goal was to remove a potentially dangerous apex-forward stable trim point while maintaining the apex-aft trim point and improving the performance of the vehicle. The optimization effort resulted in removing the apex-forward trim point while maintaining robust apex-aft stability, resulting in a vehicle with a single trim point with improved cross-range performance. The optimized CM has a larger base radius, a larger included cone angle, and a smaller corner radius than the baseline Apollo CM.

Prior to the optimization effort, a parametric study that varied each of the four vehicle-defining design variables over a range of 5 values was used to assess the design space and provide a method to corroborate the optimization results. It is rarely feasible to explore the design space, but with only four design variables it was possible. The optimization effort required only 7% of the CPU time that was needed for the parametric study to arrive at an optimum that was within 0.1% of the optimum found using the parametric study approach.

The optimization results were validated via independent Navier–Stokes computations for several design conditions, and these results confirmed that the optimized vehicle achieved the single apex-aft trim point. Navier–Stokes data corroborated the inviscid Euler computational data.

Euler computations were performed on 10 capsules that varied the four capsule-defining parameters to produce 10 geometrically similar configurations. These computations were compared with wind

tunnel test data from numerous test facilities where full-scale test models were used. The Euler CFD comparisons were performed for a wide range of Mach numbers: 0.4, 0.7, 1.2, 1.65, 3.26, 3.27, and 5.0. The computational angles of attack ranged from 0 to 180 degrees with 5-degree increments. The comparisons showed the Euler methods are capable of predicting the differences in moment coefficient data between geometrically similar objects; thus the increments between the experimental data of pairs of very similar models compare well with the increments computed by the Euler predictions. The actual values of the pitching moment also compare well at the supersonic and hypersonic Mach numbers, but the agreement lessened as the Mach number decreased for the subsonic Mach number comparisons.

REFERENCES

1. Jameson, Antony; and Baker, Timothy J.: Improvements to the Aircraft Euler Method. AIAA Paper 87-0353, presented at the 25th AIAA Aerospace Sciences Meeting, Reno, Nev., Jan. 1987.

2. http://www.sbsi-sol-optimize.com/asp/sol_product_npsol.htm

3. Zuniga, F.; Cliff, S.; Kinney, D.; Smith, S.; Hawke, V.; and Tang, C.: Vehicle Design of a Sharp CTV Concept Using a Virtual Flight Rapid Integration Test Environment. AIAA Paper 2002-4881, presented at the AIAA Atmospheric Flight Mechanics Conference and Exhibit, Monterey, Calif., Aug. 2002.

4. Cliff, S. E.; Thomas, S. D.; Baker, T. J.; Jameson, A.; and Hicks, R. M.: Aerodynamic Shape Optimization Using Unstructured Grid Method. AIAA Paper No. 02-5550, presented at the 9th Symposium on Multidisciplinary Analysis and Optimization, Atlanta, Ga., Sept. 2002.

5. Baker, T. J.; and Vassberg, J. C.: Tetrahedral Mesh Generation and Optimization. Proceedings of the 6th International Conference on Numerical Grid Generation, International Society of Grid Generation (ISGG), Mississippi State Univ., 1998, pp. 337–349.

6. Mosely, William C.; and Redd, Bass: Aerodynamic Stability Characteristics of the Apollo Launch Escape Vehicle (LEV) with Canard Surfaces Deployed. NASA TN D-4280, 1967.

7. Mosely, William C.; Graham, Ralph E.; and Hughes, Jack E.: Aerodynamic Stability Characteristics of the Apollo Command Module. NASA TN D-4688, 1968.

8. Jespersen, D. C.; Pulliam, T. H.; and Buning, P. G.: Recent Enhancements to OVERFLOW. AIAA Paper 97-0644, Jan. 1997.

9. Klopfer, G. H.; Hung, C. H.; Van der Wijngaart, R. F.; and Onufer, J. T.: A Diagonalized Diagonal Dominant Alternating Direction Implicit (D3ADI) Scheme and Subiteration Correction. AIAA Paper 98-2824, June 1998.

10. Aftosmis, M. J.; Berger, M. J.; and Melton, J. E.: Robust and Efficient Cartesian Mesh Generation for Component-Based Geometry. AIAA Paper No. 97-0196.

11. Jameson, Antony; Shankaran, Sriram; Martinelli, Luigi; Cliff, Susan; and Thomas, Scott: Aerodynamic Shape Optimization. AIAA Paper No. 2005-1013, presented at the 43rd AIAA Aerospace Sciences Meeting, Reno, Nev., Jan. 2005.

Table 1. Geometry description of CMs with experimental data for comparison with computational data.

Apollo Command Module	θ, deg.	R_A, in.	R_C, in.	R_O, in.
C01	33	15.4	7.7	184.8
C02	33	9.152	7.7	184.8
C03	33	9.152	0.0	184.8
C04	33	9.152	15.4	184.8
C05	33	9.152	23.1	184.8
C06	33	9.152	7.7	154.0
C07	33	9.152	7.7	215.6
C08	30	9.152	7.7	184.8
C09	36	9.152	7.7	184.8
C10	40	9.152	7.7	184.8

Table 2. Four-dimensional matrix of objective function value multiplied by 1000 and rounded to the nearest integer.

	θ = 25					θ = 30					θ = 35					θ = 40					θ = 45				
	289	369	491	658	888	89	106	136	185	261	89	91	99	113	139	117	120	129	138	150	142	153	168	186	201
	245	319	430	591	807	70	87	115	160	229	59	66	78	94	118	67	80	97	113	130	73	94	123	151	175
R_A = 5	247	319	426	582	793	69	86	112	156	223	53	60	72	88	113	56	69	87	105	123	56	77	109	140	168
	250	322	428	581	793	72	87	113	155	220	52	59	70	86	110	54	65	83	102	121	53	71	103	136	164
	255	327	430	580	786	75	89	113	154	220	54	59	69	85	109	55	63	80	100	119	54	69	99	133	163
	299	379	502	671	905	90	107	138	188	263	88	90	98	112	137	115	119	127	137	149	141	152	168	184	199
	254	329	444	606	823	72	89	117	163	233	59	66	77	93	117	67	79	96	112	129	72	94	122	150	174
R_A = 10	257	330	441	595	810	71	88	115	159	227	52	60	72	88	112	55	68	86	104	123	56	77	108	140	166
	262	333	441	595	807	74	89	115	159	224	52	59	70	86	110	53	64	81	101	119	53	71	101	134	163
	265	338	445	596	805	76	91	115	158	223	54	59	69	84	108	54	62	79	98	118	53	68	98	131	161
	311	395	521	695	924	92	109	142	192	269	87	89	97	112	137	114	118	125	134	147	139	149	166	183	198
	270	349	462	624	846	74	92	120	168	238	57	65	77	92	117	66	77	94	111	127	71	92	121	149	172
R_A = 15	271	349	460	618	834	73	91	119	164	233	51	59	71	87	112	54	66	84	102	121	55	76	107	138	165
	275	352	462	618	829	76	93	119	162	230	51	58	69	85	109	52	62	80	99	117	52	70	100	132	161
	280	357	466	615	826	79	95	120	163	229	54	58	68	84	108	53	61	78	97	116	52	67	97	130	159
	331	416	543	715	949	95	113	146	198	276	85	87	96	110	138	111	115	123	132	145	139	147	163	180	195
	290	368	487	649	871	78	96	126	173	246	56	64	76	92	117	64	76	92	108	124	69	91	119	147	169
R_A = 20	291	370	480	643	862	77	96	124	171	241	51	59	71	87	112	53	64	82	100	118	54	74	105	135	161
	295	374	485	642	857	81	98	125	170	239	51	58	69	85	110	51	61	78	96	115	51	68	98	130	158
	300	378	488	643	853	84	100	126	169	238	53	58	68	84	108	52	59	75	94	114	51	65	95	127	156
	354	439	569	747	982	99	118	152	205	284	83	86	95	110	136	109	112	119	130	142	136	146	161	177	192
	311	393	512	679	905	82	102	132	182	256	56	63	75	92	117	62	73	89	105	122	68	88	116	144	166
R_A = 25	312	393	511	673	894	82	102	132	179	250	50	58	70	87	112	51	63	79	98	115	53	72	102	133	159
	318	398	516	672	889	85	104	131	178	247	51	58	68	85	110	49	59	75	94	113	50	66	95	127	155
	323	403	517	675	888	90	107	133	178	247	53	58	68	83	109	51	58	73	92	111	50	64	92	125	154

Table 3. Defining parameters for baseline and designed Apollo Command Modules.

	θ, degrees	R_A, in.	R_C, in.	R_O, in.
Baseline C01	33.0	15.4	7.7	184.8
Best Parametric	40.0	25.0	0.0	331.25
First Optimized	35.6	14.17	0.0	297.8
Second Optimized	44.99	14.18	0.0	385.4
Third Optimized	45.0	16.0	5.0	400.0

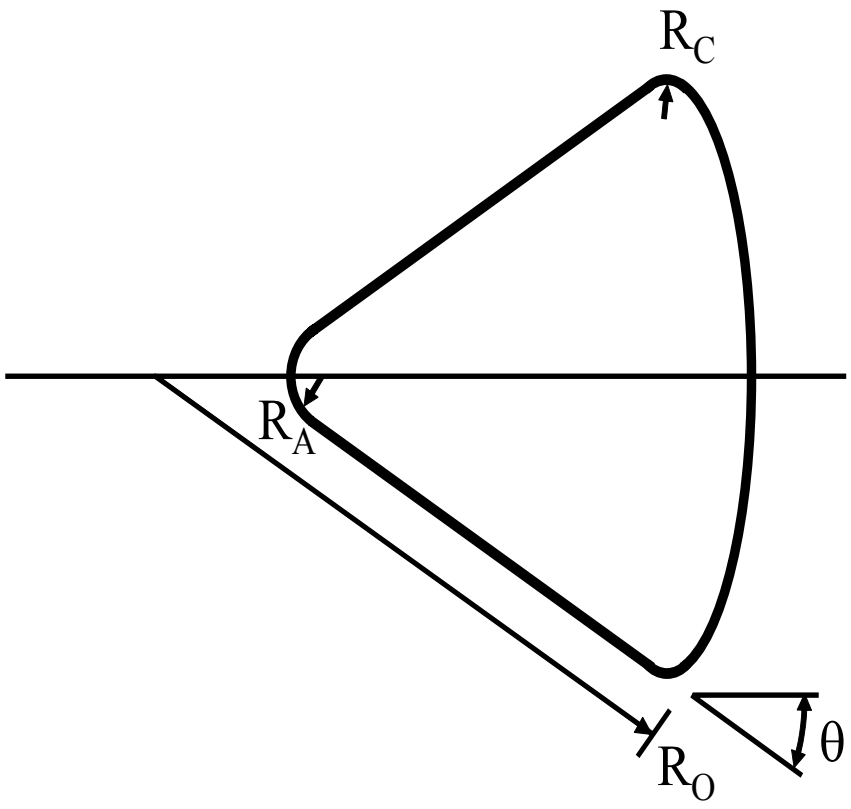

Figure 1. Variables used to change the shape of the capsule.

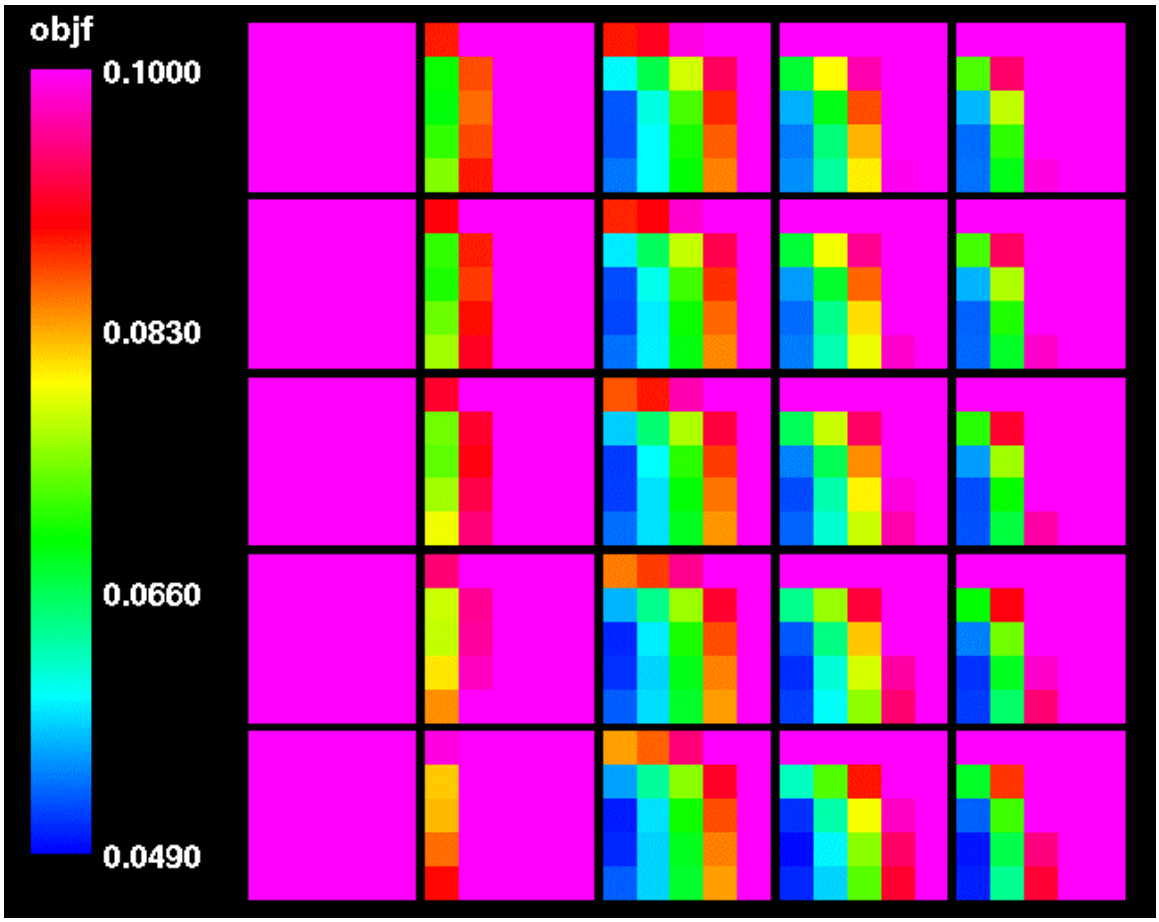

Figure 2. Parametric results of the objective function in the four-dimensional matrix in table 2. Color determined by the value of objective function.

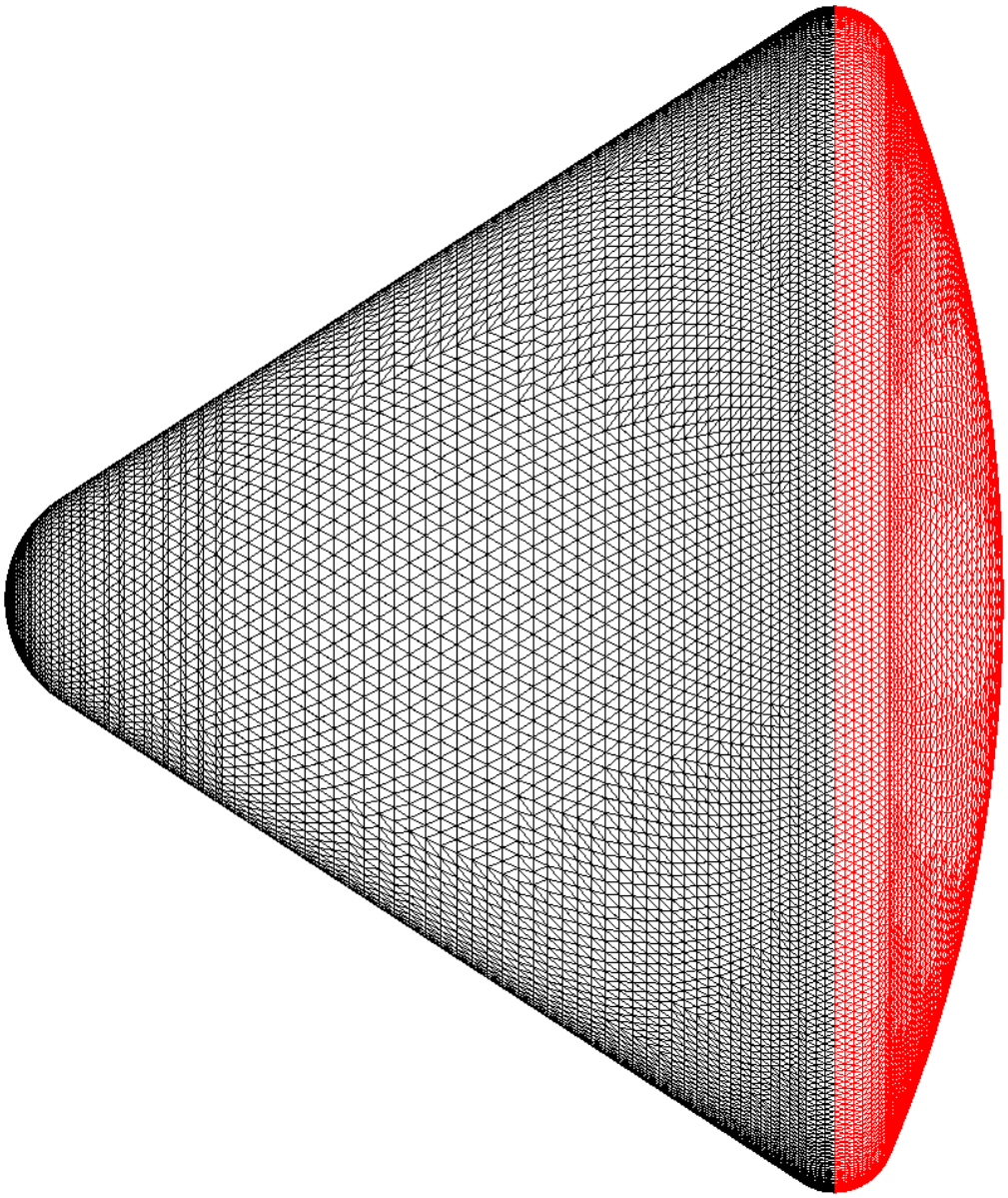

Figure 3. Baseline C01 Apollo Command Module unstructured surface mesh, showing apex, cone, and corner to waist in black, then corner aft of waist and base in red. This and the next four pictures are made with orthographic projection.

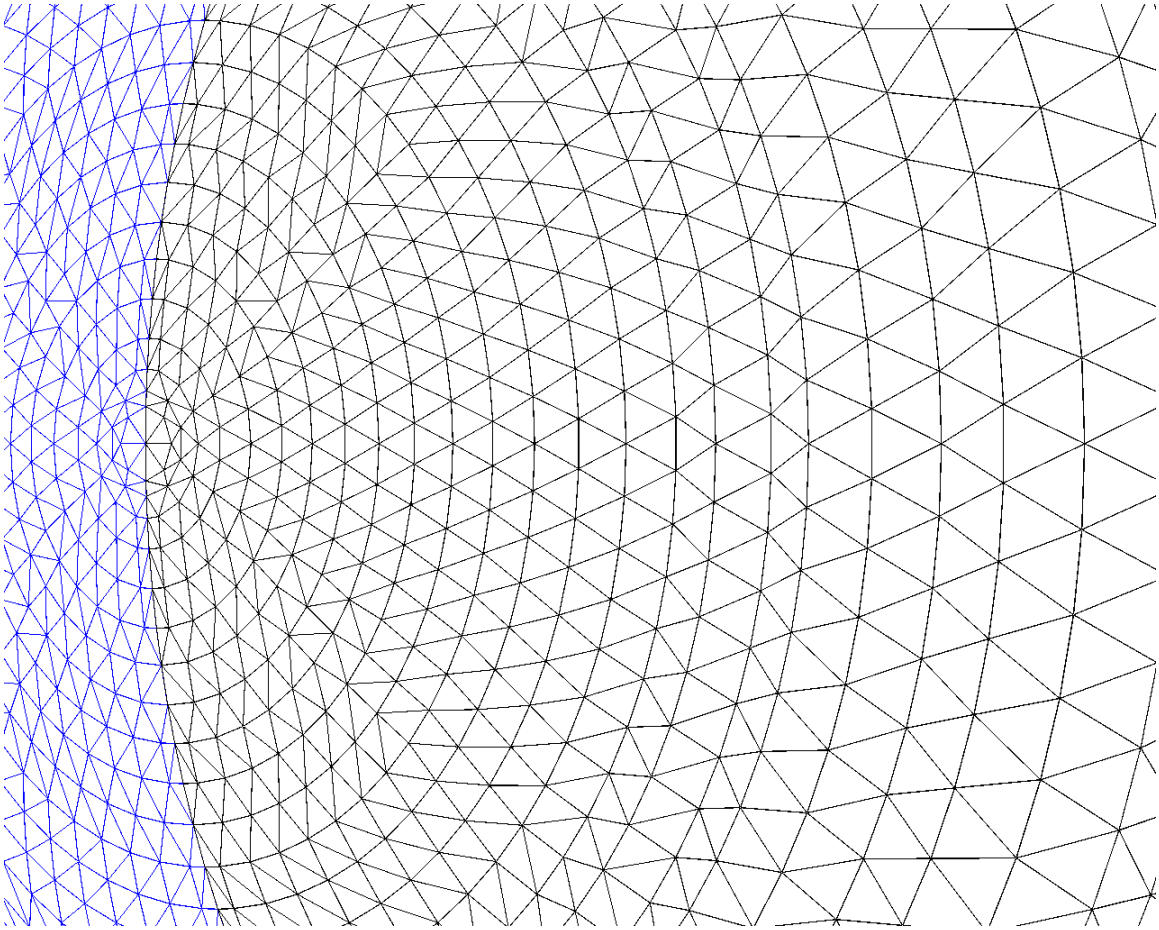

Figure 4. Baseline C01 Apollo Command Module unstructured surface mesh near the nose point of the apex. A mirror image is shown in blue.

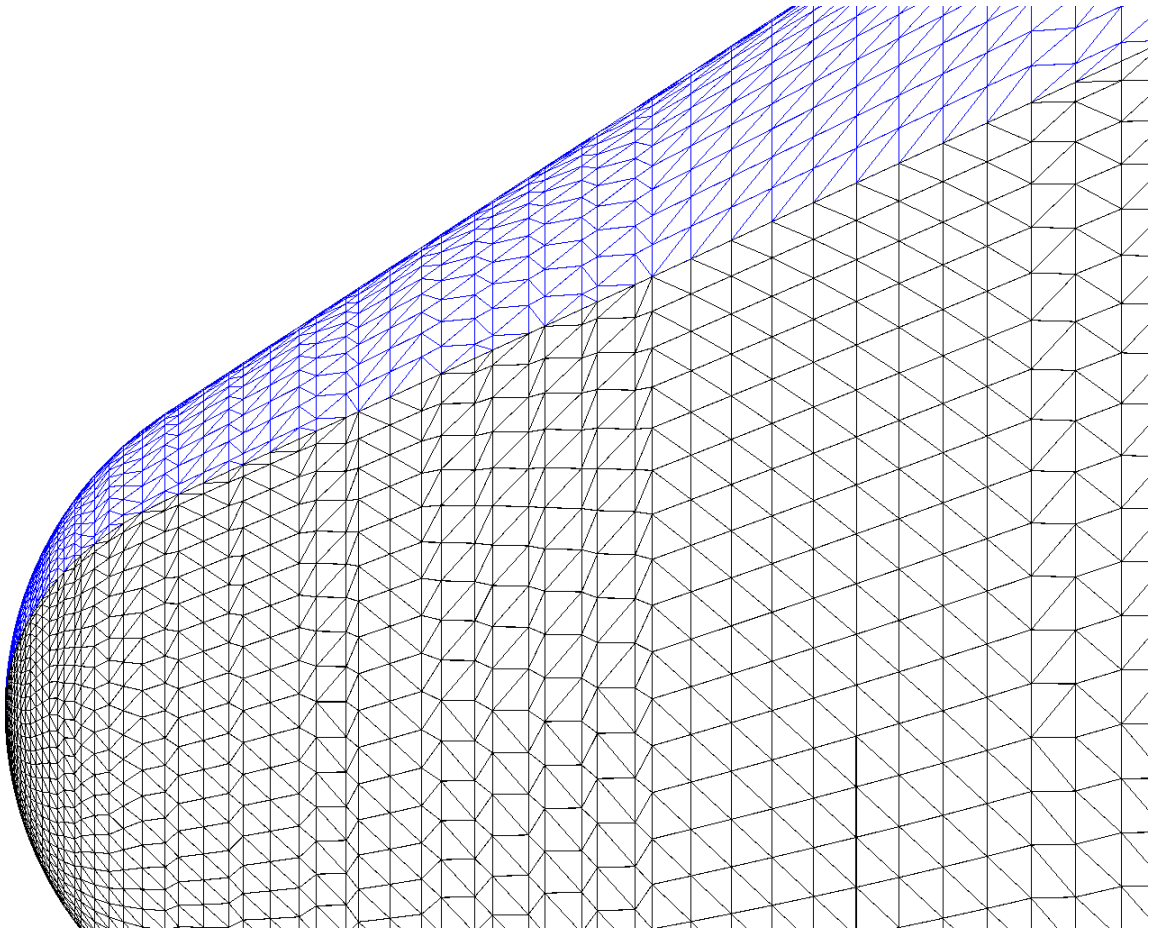

Figure 5. Baseline C01 Apollo Command Module unstructured surface mesh showing the apex and forward cone. A mirror image is shown in blue.

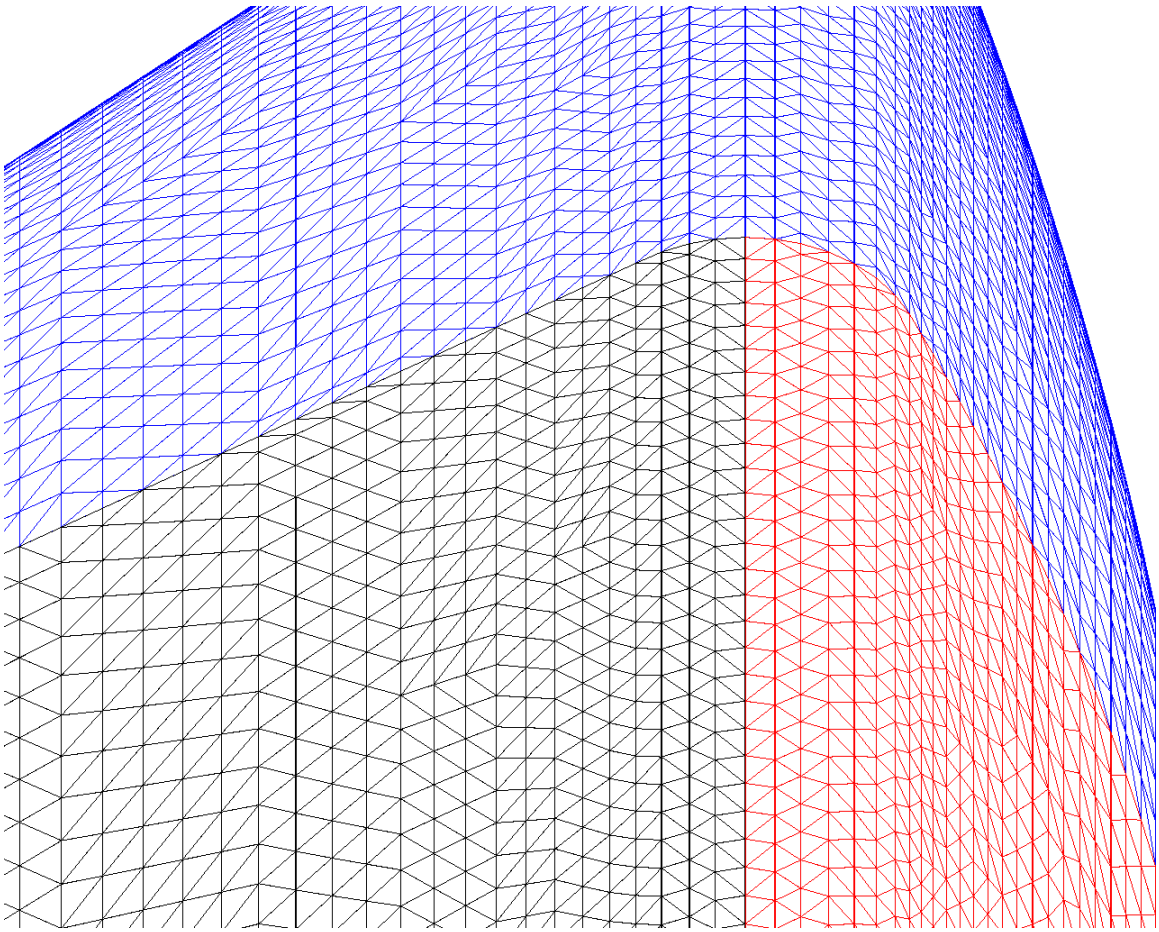

Figure 6. Baseline C01 Apollo Command Module unstructured surface mesh showing the aft cone and a portion of the corner to the waist in black, then the rest of the corner and the base in red. A mirror image is shown in blue.

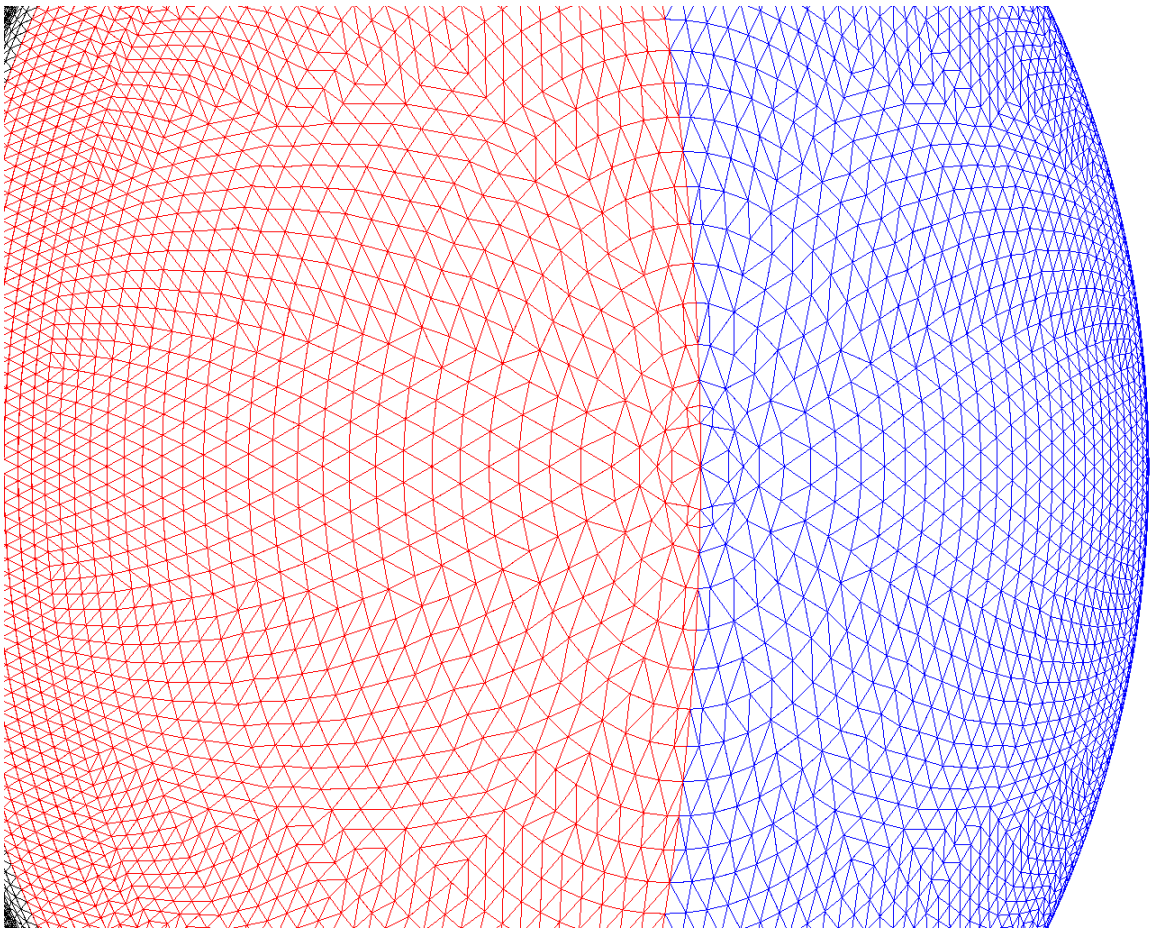

Figure 7. Baseline C01 Apollo Command Module unstructured surface mesh showing the forward corner in black, then aft of the waist the corner and base is red, with a mirror image in blue.

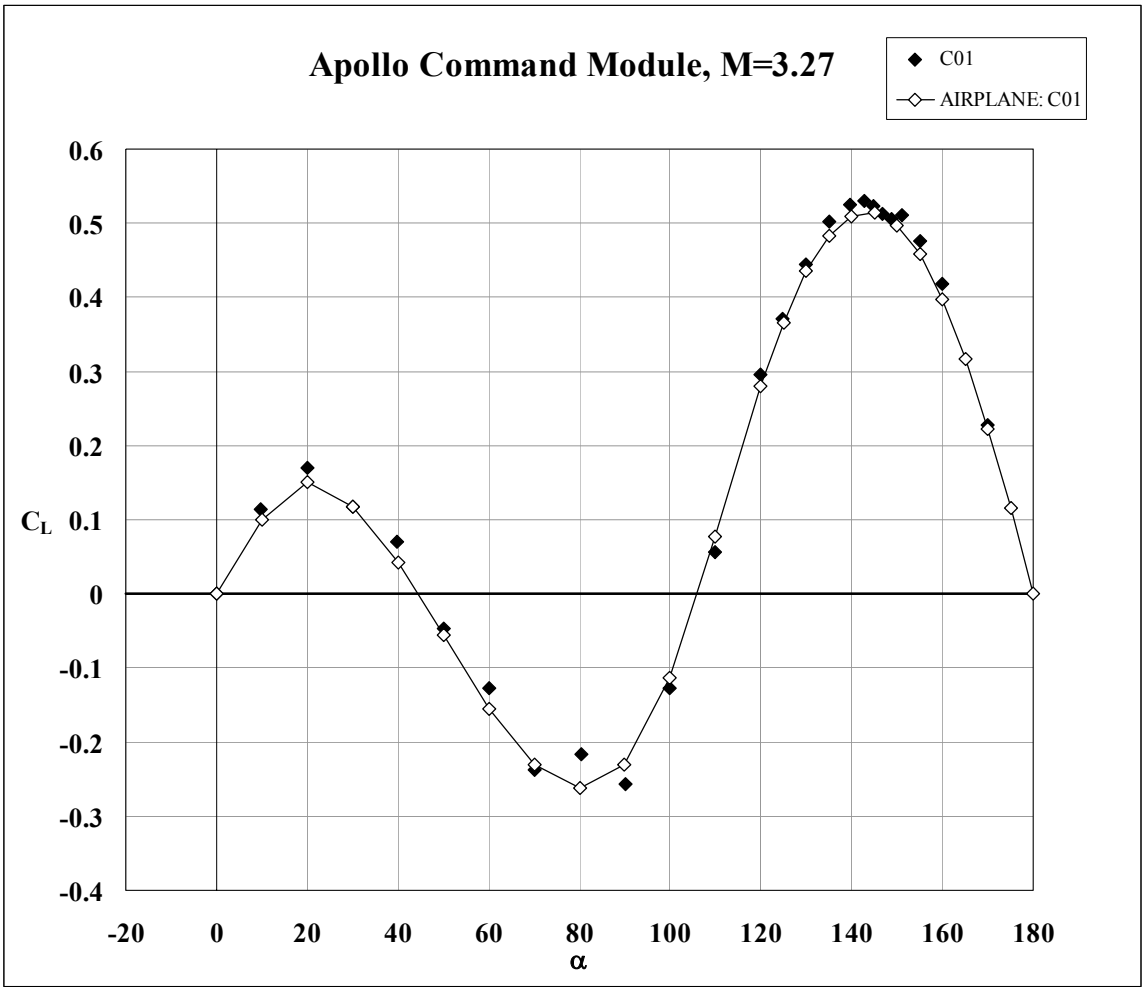

Figure 8. Lift coefficient data of the Apollo Command Module (C01) configuration. AIRPLANE computations and experiment.

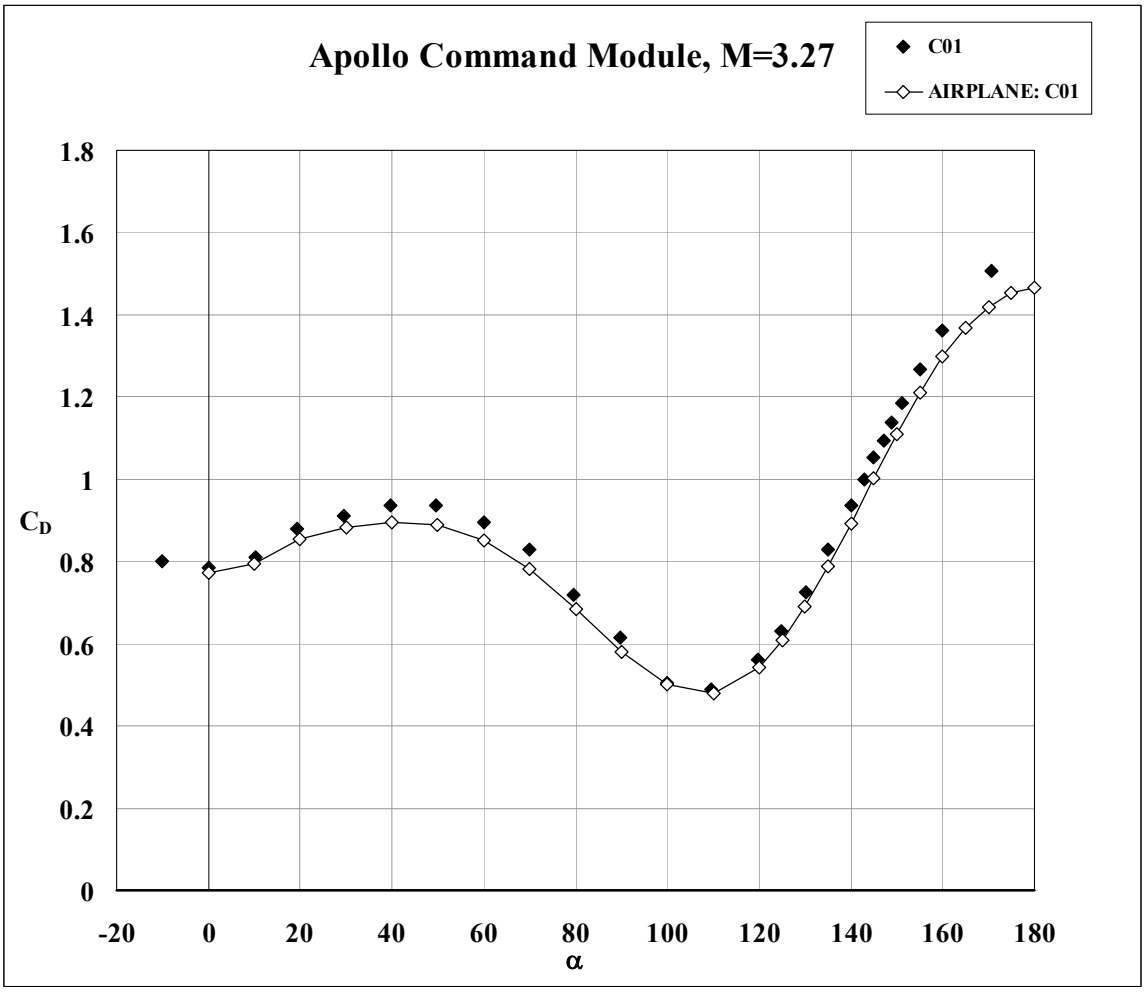

Figure 9. Drag coefficient data of the Apollo Command Module (C01) configuration. AIRPLANE computations and experiment.

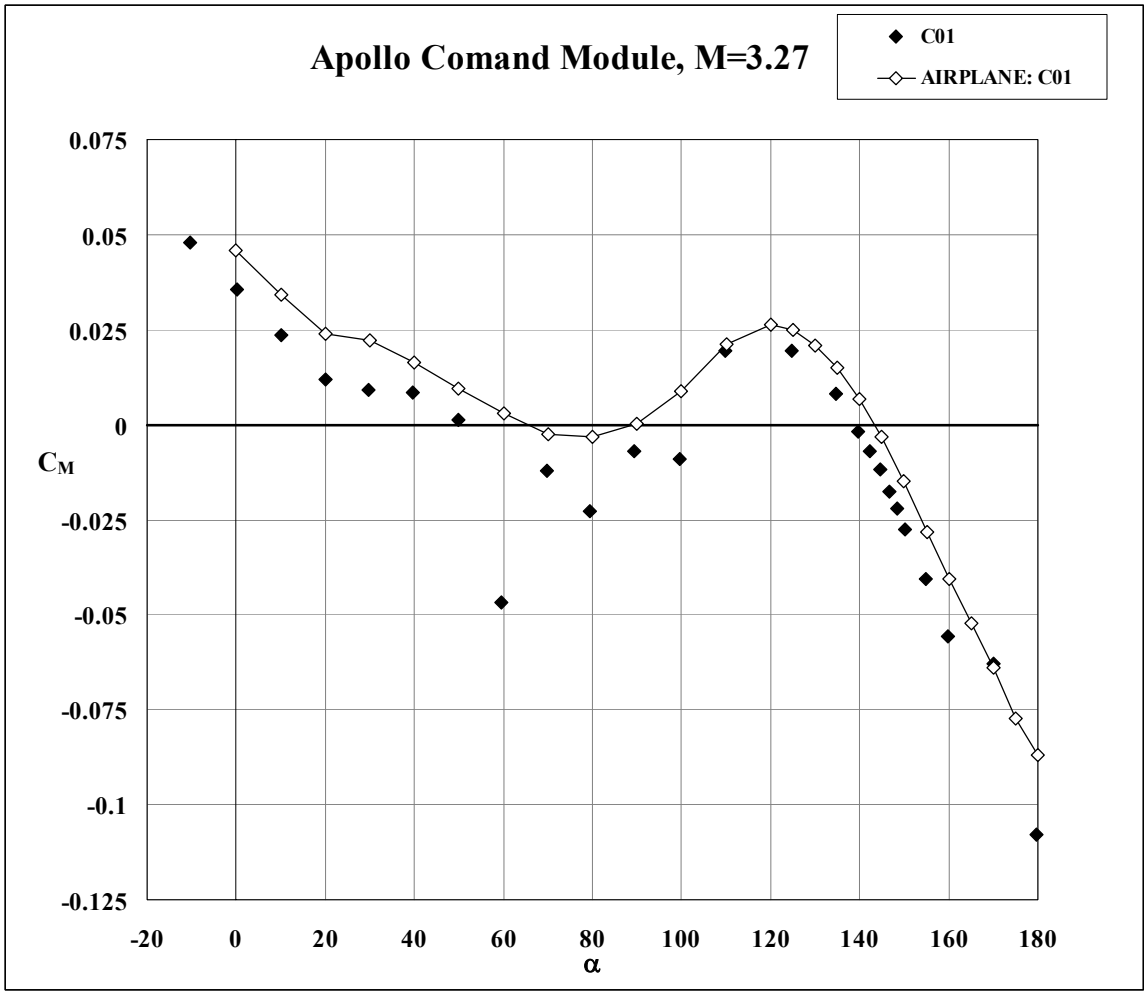

Figure 10. Pitching moment coefficient data of the Apollo Command Module (C01) configuration. AIRPLANE computations and experiment.

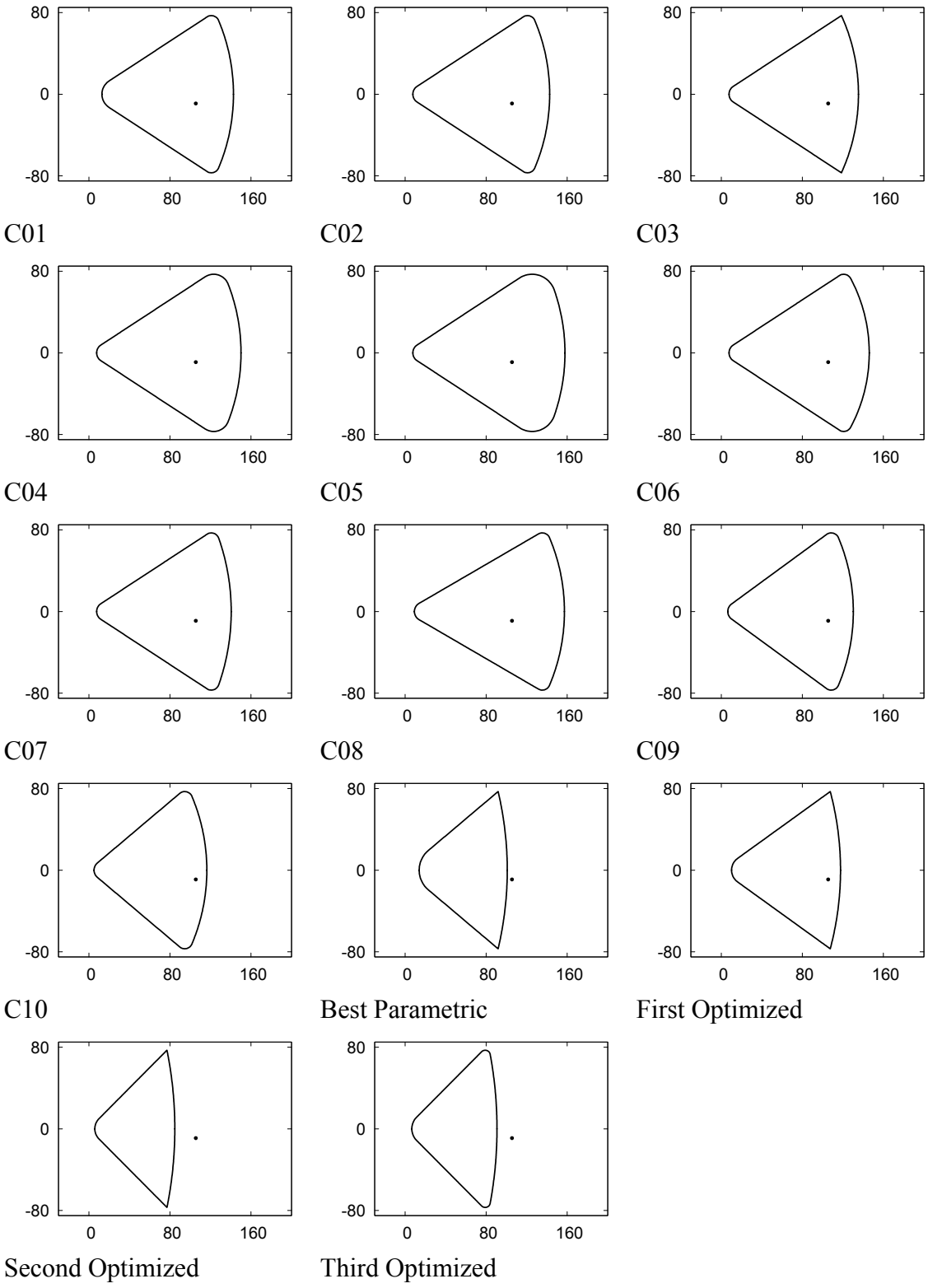

Figure 11. Apollo Command Module profiles, showing nominal center of gravity.

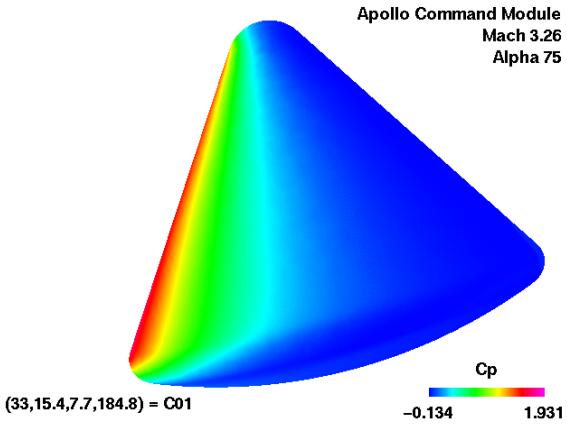

Figure 12. Baseline C01 at $\alpha = 75$.

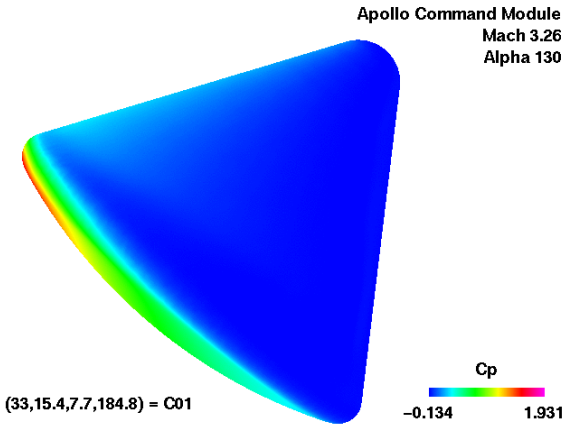

Figure 13. Baseline C01 at $\alpha = 130$.

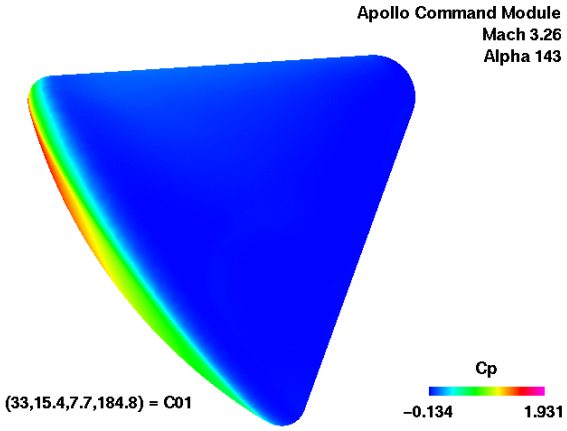

Figure 14. Baseline C01 at $\alpha = 143$.

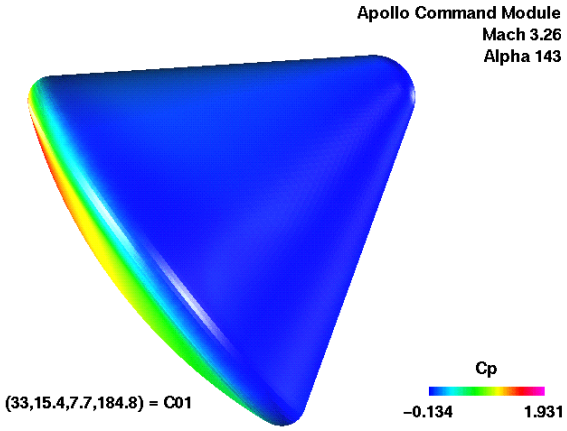

Figure 15. Baseline C01 at trim, $\alpha = 143$.

Figures 12, 13, 14, and 15. AIRPLANE predictions of Cp on the baseline C01 Apollo Command Module, Mach 3.26, at the three design-point angles of attack (75, 130, 143 degrees) and at base-forward trim (143 degrees, shown shaded with two lights). The 4-tuple $(\theta, R_A, R_C, R_O) = (33, 15.4, 7.7, 184.8)$ defines the baseline C01 Apollo Command Module.

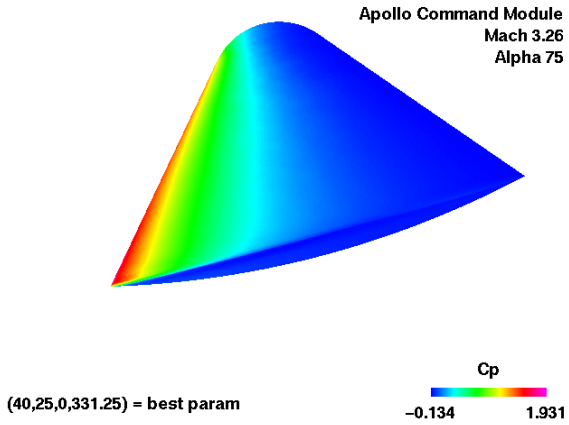

Figure 16. Best Parametric at α = 75.

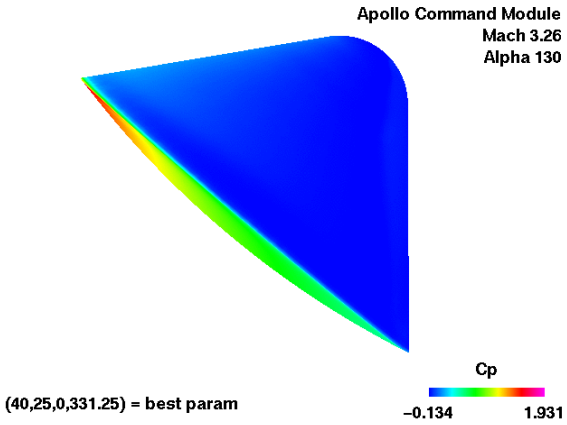

Figure 17. Best Parametric at α = 130.

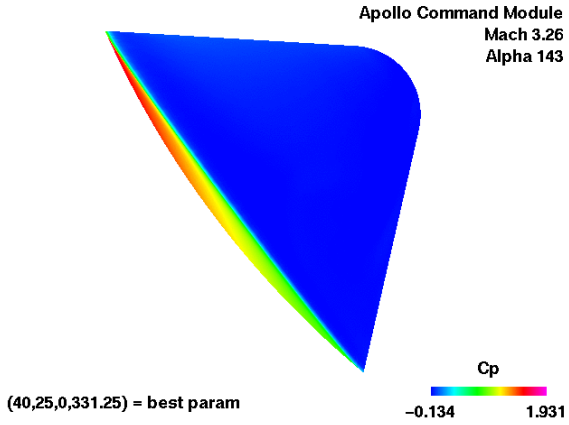

Figure 18. Best Parametric at α = 143.

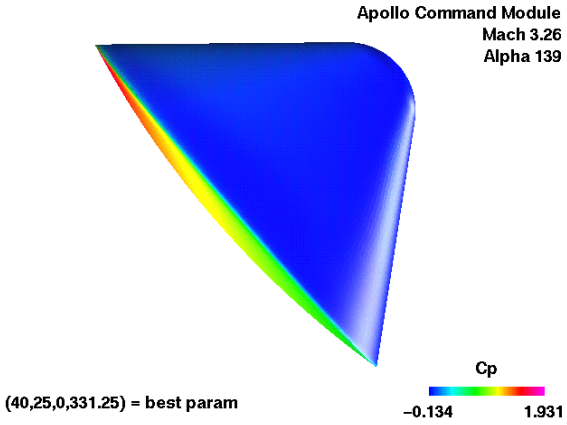

Figure 19. Best Parametric, trim, α = 139.

Figures 16, 17, 18, and 19. AIRPLANE predictions of Cp on the Best Parametric Apollo Command Module, Mach 3.26, at the three design-point angles of attack (75, 130, 143 degrees) and at base-forward trim (139 degrees, shown shaded with two lights). The 4-tuple (θ, R_A, R_C, R_O) = (40, 25, 0, 331.25) defines the best parametric shape using the first objective function.

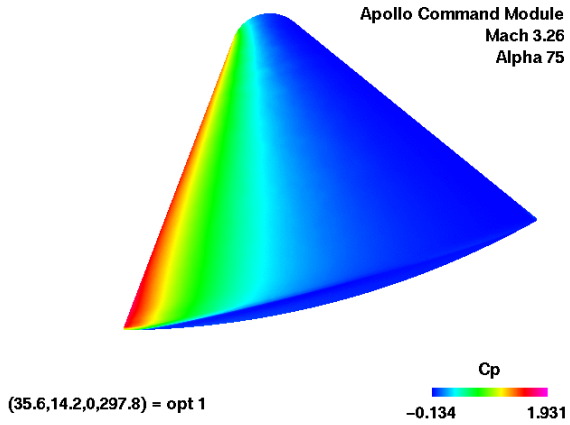

Figure 20. First Optimized at α = 75.

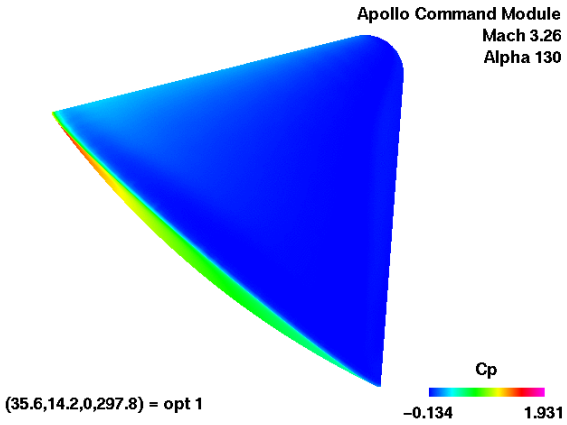

Figure 21. First Optimized at α = 130.

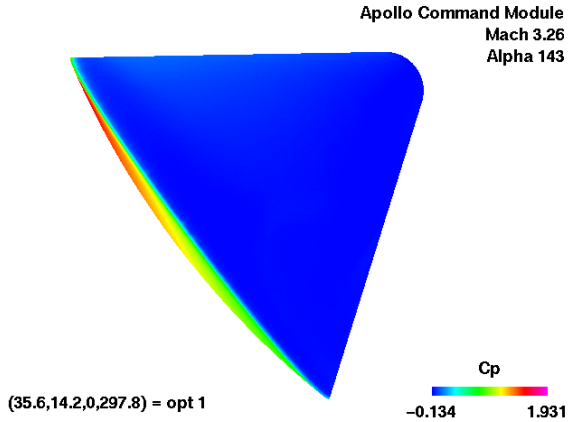

Figure 22. First Optimized at α = 143.

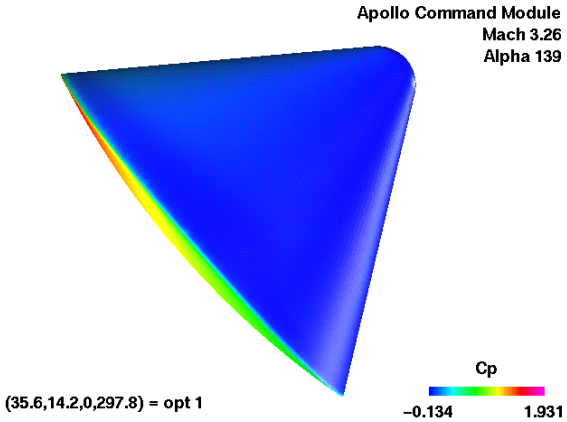

Figure 23. First Optimized, trim, α = 139.

Figures 20, 21, 22, and 23. AIRPLANE predictions of Cp on the First Optimized Apollo Command Module, Mach 3.26, at the three design-point angles of attack (75, 130, 143 degrees) and at base-forward trim (139 degrees, shown shaded with two lights). The 4-tuple (θ, R_A, R_C, R_O) = (35.6, 14.2, 0, 297.8) defines the first optimized shape using the first objective function.

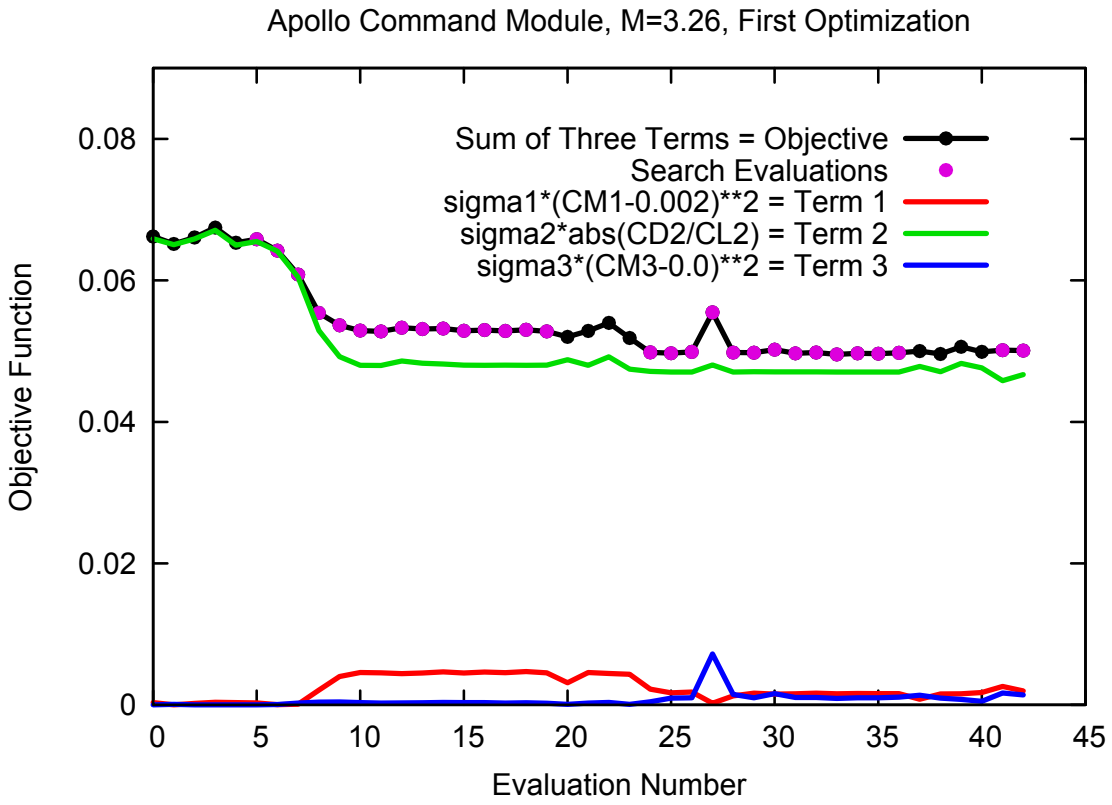

Figure 24. NPSOL objective function history for the first optimization of the Apollo Command Module, Mach 3.26. Black dots indicate numerical approximations of partial derivatives. Numbering starts at 0.

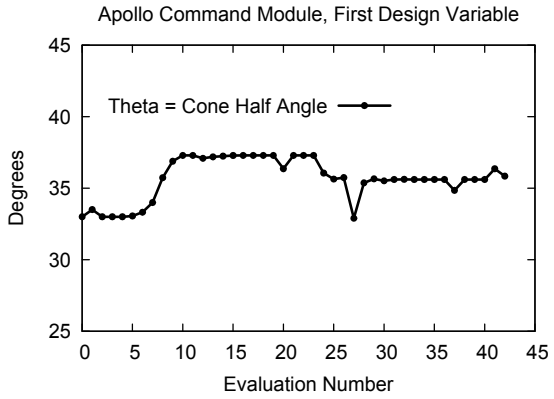

Figure 25. Cone Half Angle History.

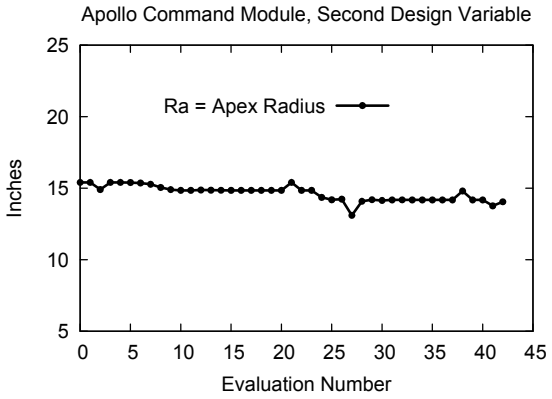

Figure 26. Apex Radius History.

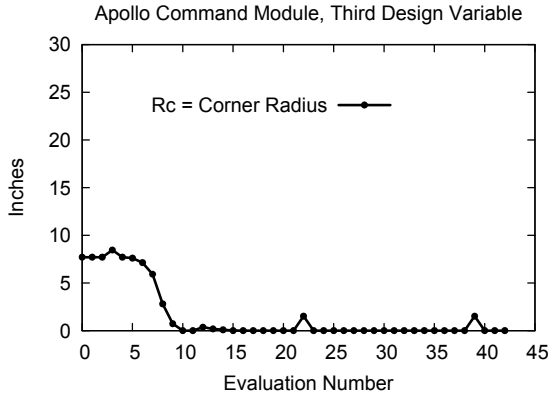

Figure 27. Corner Radius History.

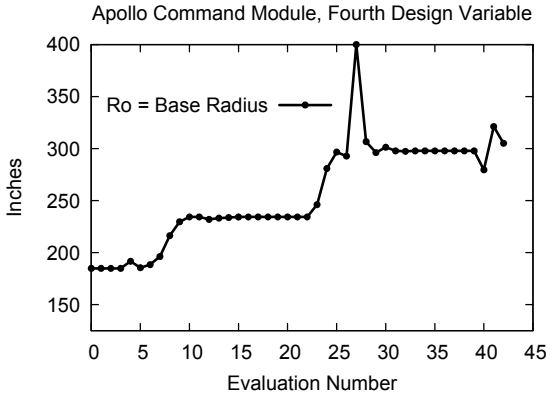

Figure 28. Base Radius History.

Figures 25, 26, 27, and 28. Design parameter values at each objective function evaluation for the first NPSOL optimization, Mach 3.26. The initial 4-tuple (θ, R_A, R_C, R_O) = (33, 15.4, 7.7, 184.8) defines the baseline C01 Apollo Command Module, and the optimized shape was approximately (35.6, 14.17, 0.0, 297.8).

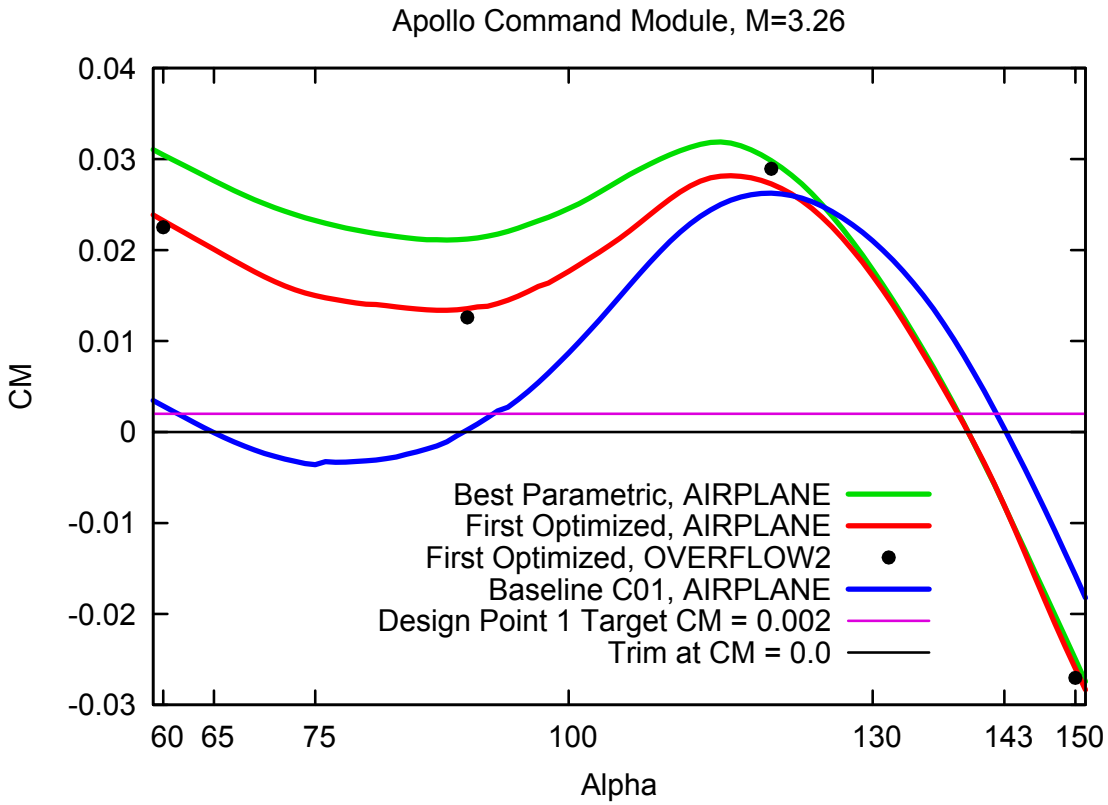

Figure 29. Pitching moment coefficient for baseline C01, best parametric and first optimized shapes, with Navier–Stokes predictions for the optimized shape (OVERFLOW2) at α = 60, 90, 120, and 150 degrees. See also figure 30.

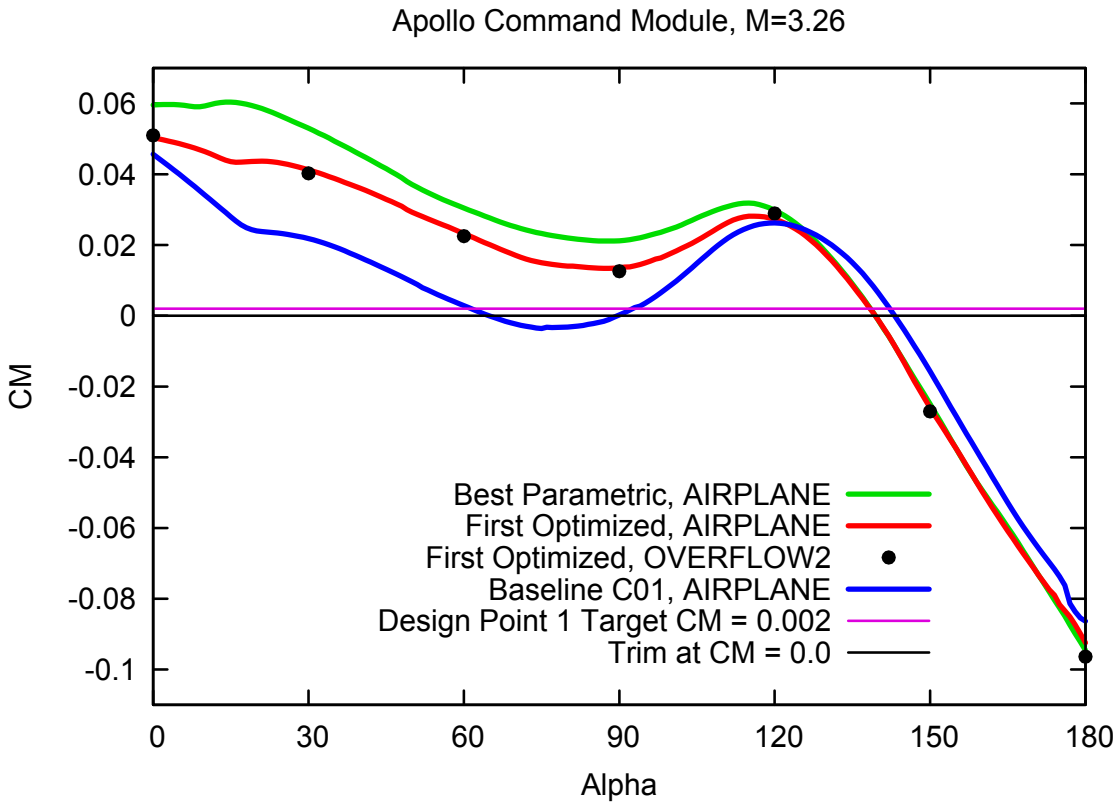

Figure 30. Alpha 0 to 180 pitching moment coefficient for baseline C01, best parametric and first optimized shapes, with Navier–Stokes predictions for the optimized shape (OVERFLOW2). Compare with figure 51.

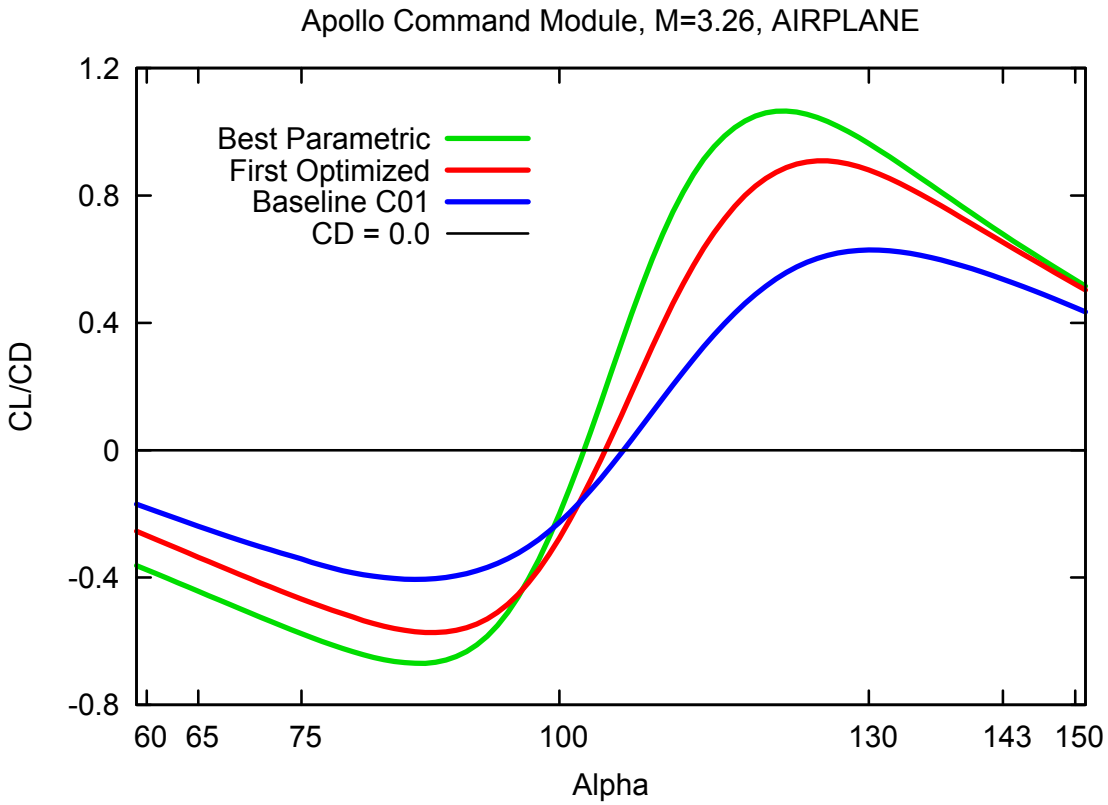

Figure 31. Lift-to-drag performance computed by AIRPLANE for baseline C01, best parametric and first optimized shapes. See also figure 32.

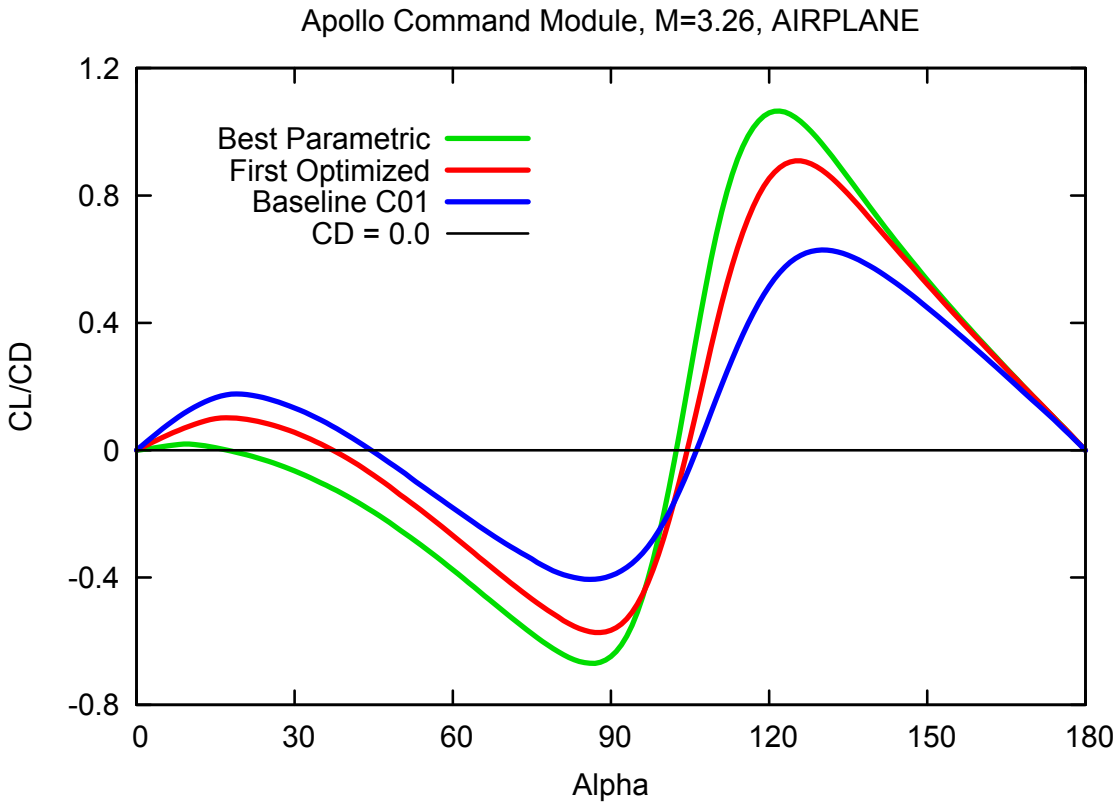

Figure 32. Alpha 0 to 180 lift-to-drag performance computed by AIRPLANE for baseline C01, best parametric and first optimized shapes. Compare with figure 52.

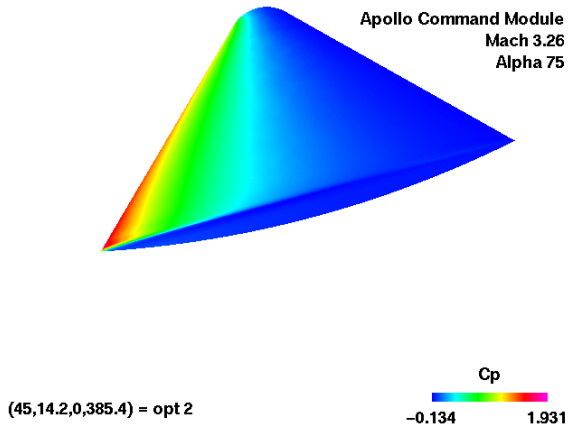

Figure 33. Second Optimized at α = 75.

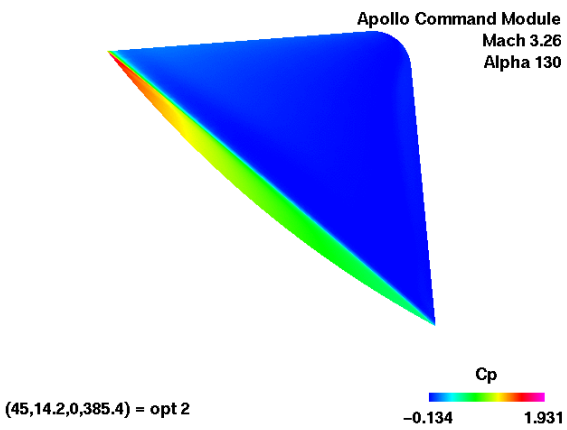

Figure 34. Second Optimized at α = 130.

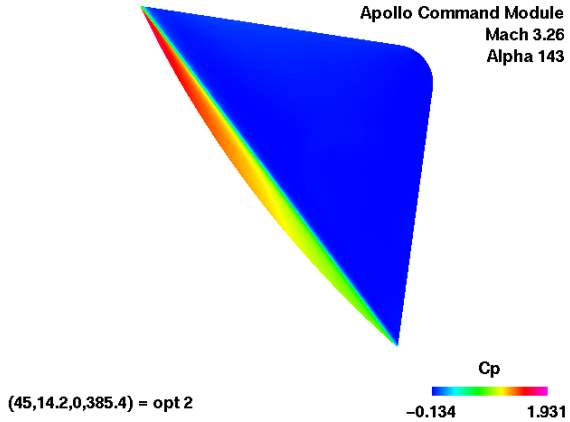

Figure 35. Second Optimized at α = 143.

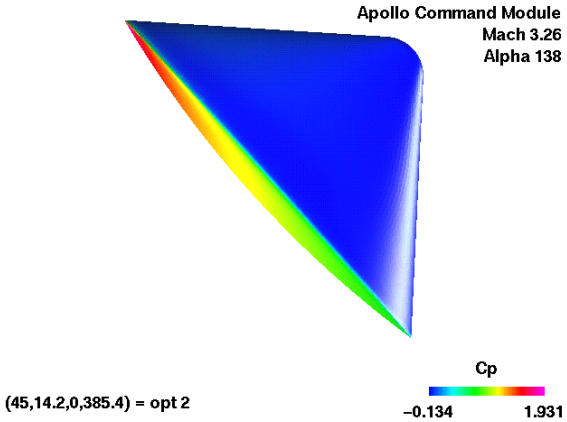

Figure 36. Second Optim., trim, α = 138.

Figures 33, 34, 35, and 36. AIRPLANE predictions of Cp on the Second Optimized Apollo Command Module, Mach 3.26, at the three design-point angles of attack (75, 130, 143 degrees) and at base-forward trim (138 degrees, shown shaded with two lights). The 4-tuple (θ, R_A, R_C, R_O) = (45, 14.2, 0, 385.4) defines the second optimized shape using the second objective function.

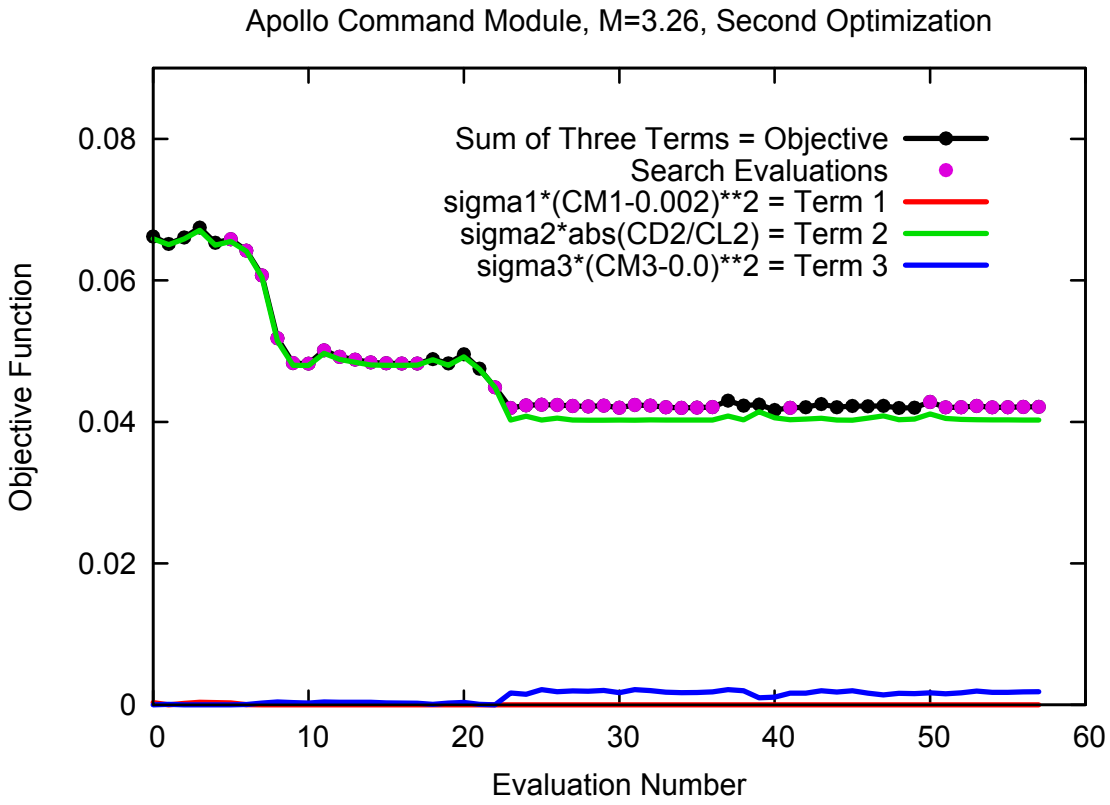

Figure 37. NPSOL objective function history for the second optimization of the Apollo Command Module, Mach 3.26. Black dots indicate numerical approximations of partial derivatives. Numbering starts at 0.

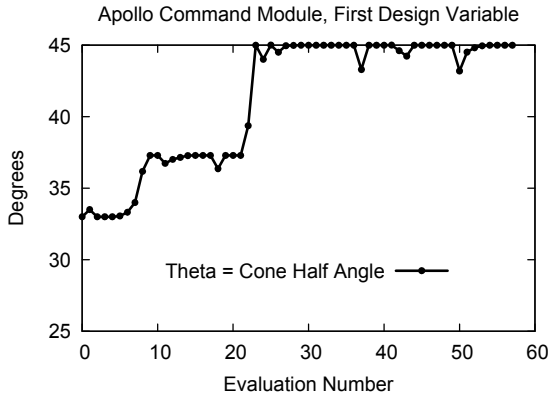

Figure 38. Cone Half Angle History.

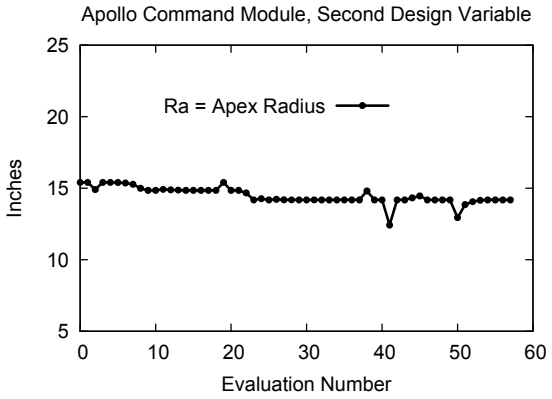

Figure 39. Apex Radius History.

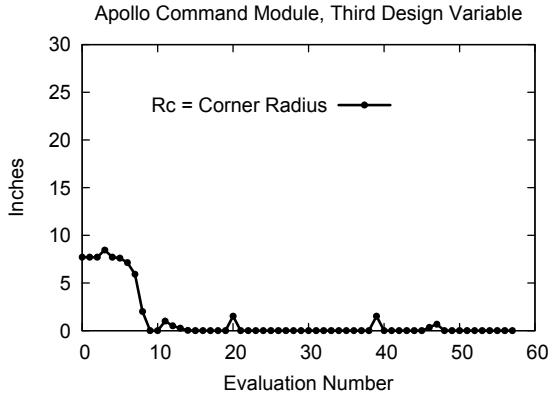

Figure 40. Corner Radius History.

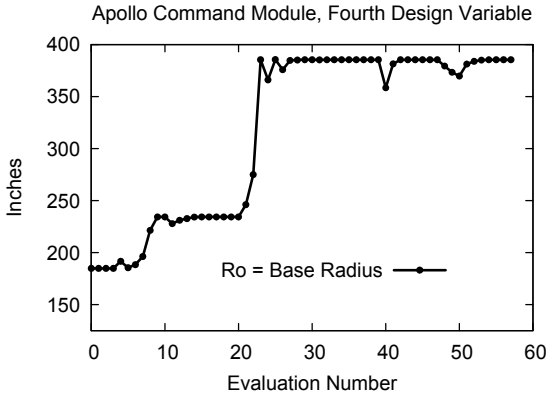

Figure 41. Base Radius History.

Figures 38, 39, 40, and 41. Design parameter values at each objective function evaluation for the second NPSOL Optimization, Mach 3.26. The initial 4-tuple (θ, R_A, R_C, R_O) = (33, 15.4, 7.7, 184.8) defines the baseline C01 Apollo Command Module, and the optimized shape was approximately (44.99, 14.18, 0.0, 385.4).

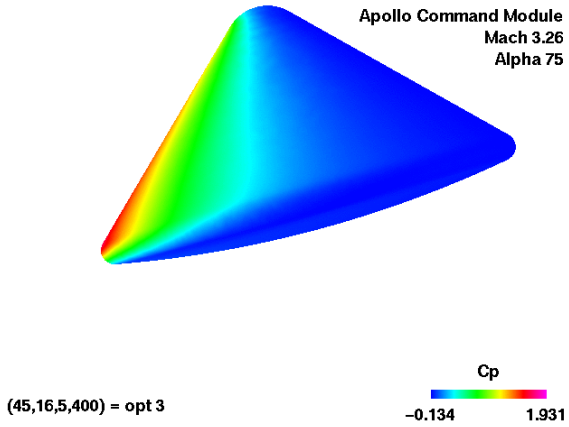

Figure 42. Third Optimized at α = 75.

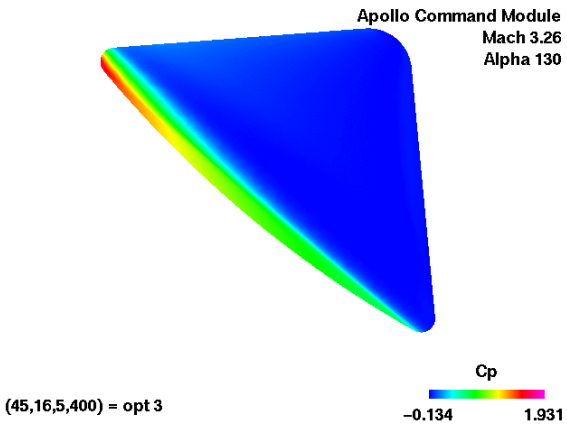

Figure 43. Third Optimized at α = 130.

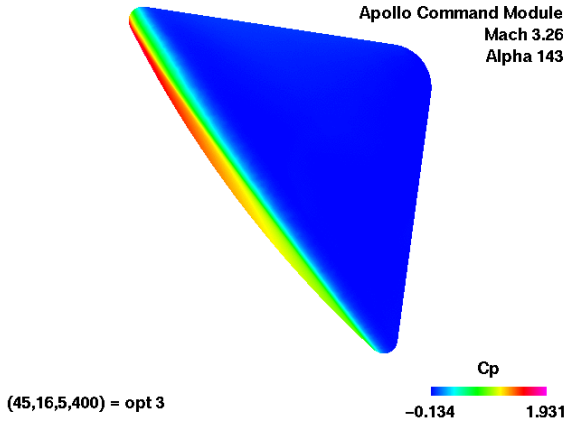

Figure 44. Third Optimized at α = 143.

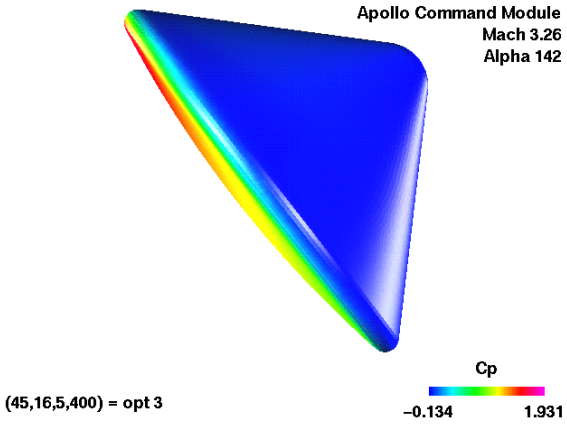

Figure 45. Third Optim., trim, α = 142.

Figures 42, 43, 44, and 45. AIRPLANE predictions of Cp on the Third Optimized Apollo Command Module, Mach 3.26, at the three design-point angles of attack (75, 130, 143 degrees) and at base-forward trim (142 degrees, shown shaded with two lights). The 4-tuple (θ, R_A, R_C, R_O) = (45, 16, 5, 400) defines the second optimized shape using the second objective function.

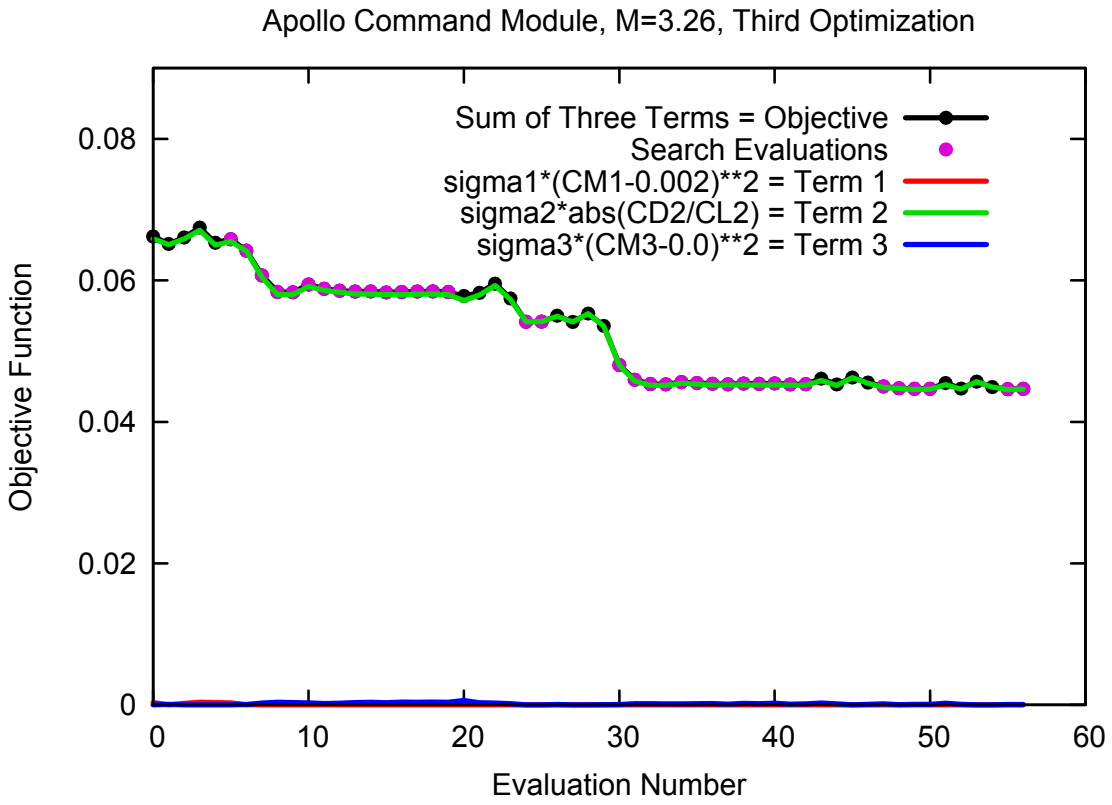

Figure 46. NPSOL objective function history for the third optimization of the Apollo Command Module, Mach 3.26. Black dots indicate numerical approximations of partial derivatives. Numbering starts at 0.

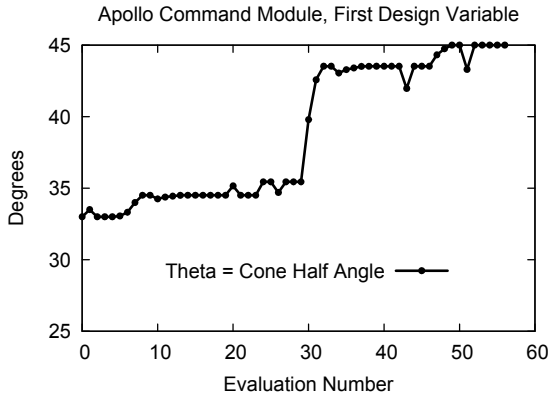

Figure 47. Cone Half Angle History.

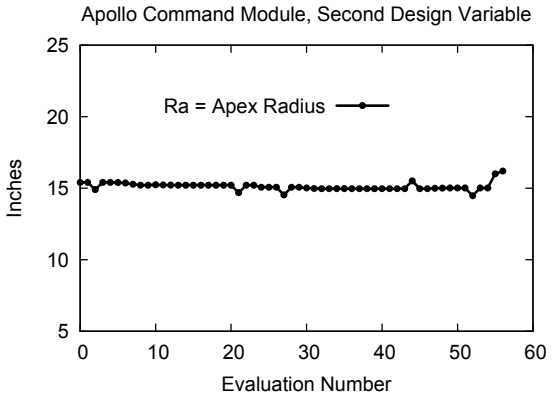

Figure 48. Apex Radius History.

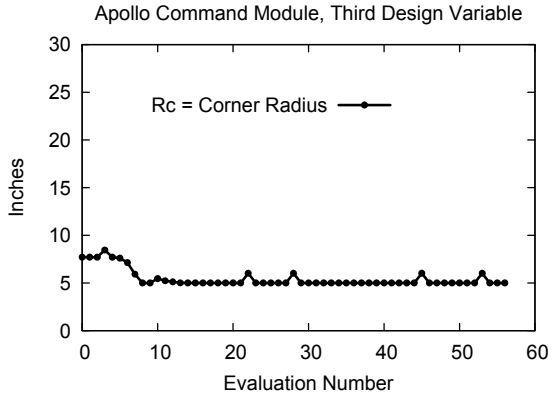

Figure 49. Corner Radius History.

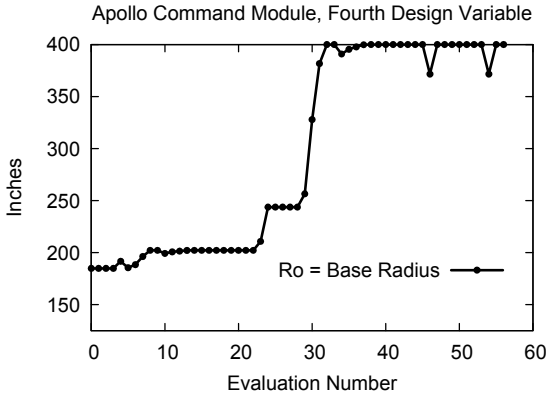

Figure 50. Base Radius History.

Figures 47, 48, 49, and 50. Design parameter values at each objective function evaluation for the third NPSOL optimization, Mach 3.26. The initial 4-tuple (θ, R_A, R_C, R_O) = (33, 15.4, 7.7, 184.8) defines the baseline C01 Apollo Command Module, and the optimized shape was approximately (45, 16, 5, 400). In this case, the lower limit for corner radius, R_C, was raised from 0 to 5 inches.

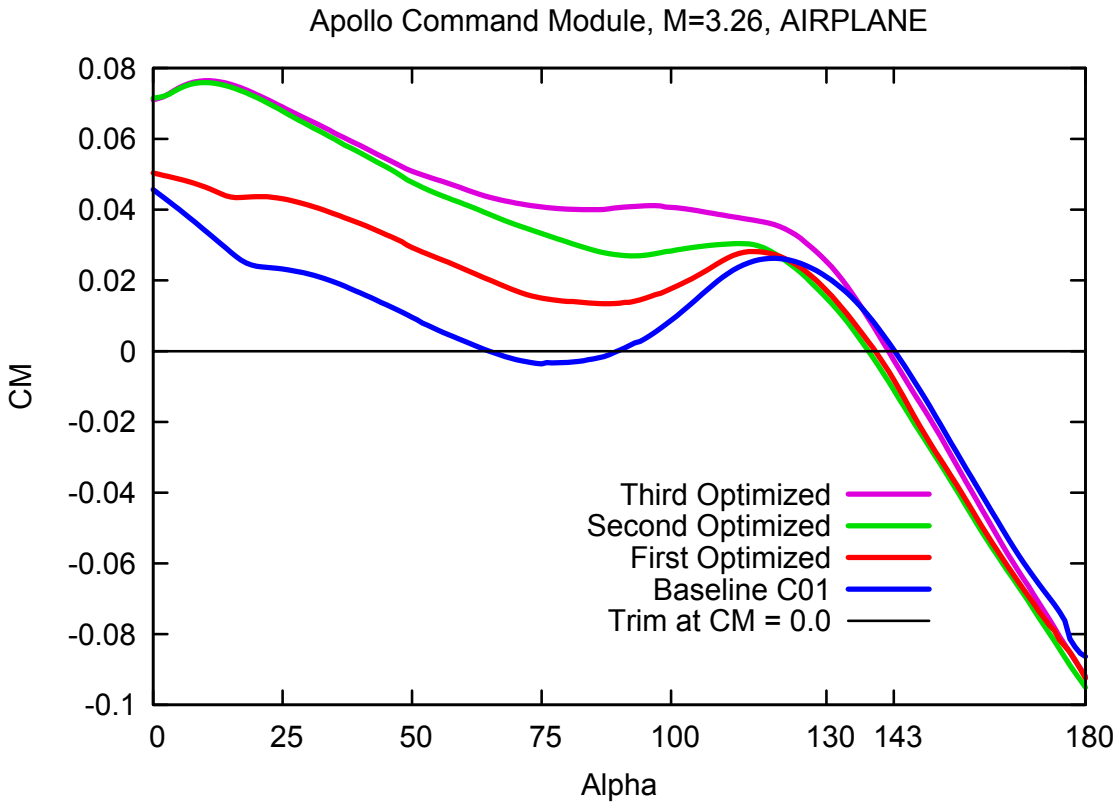

Figure 51. Alpha 0 to 180 pitching moment coefficient computed by AIRPLANE for baseline C01 and the three NPSOL optimized cases. Compare with figure 30.

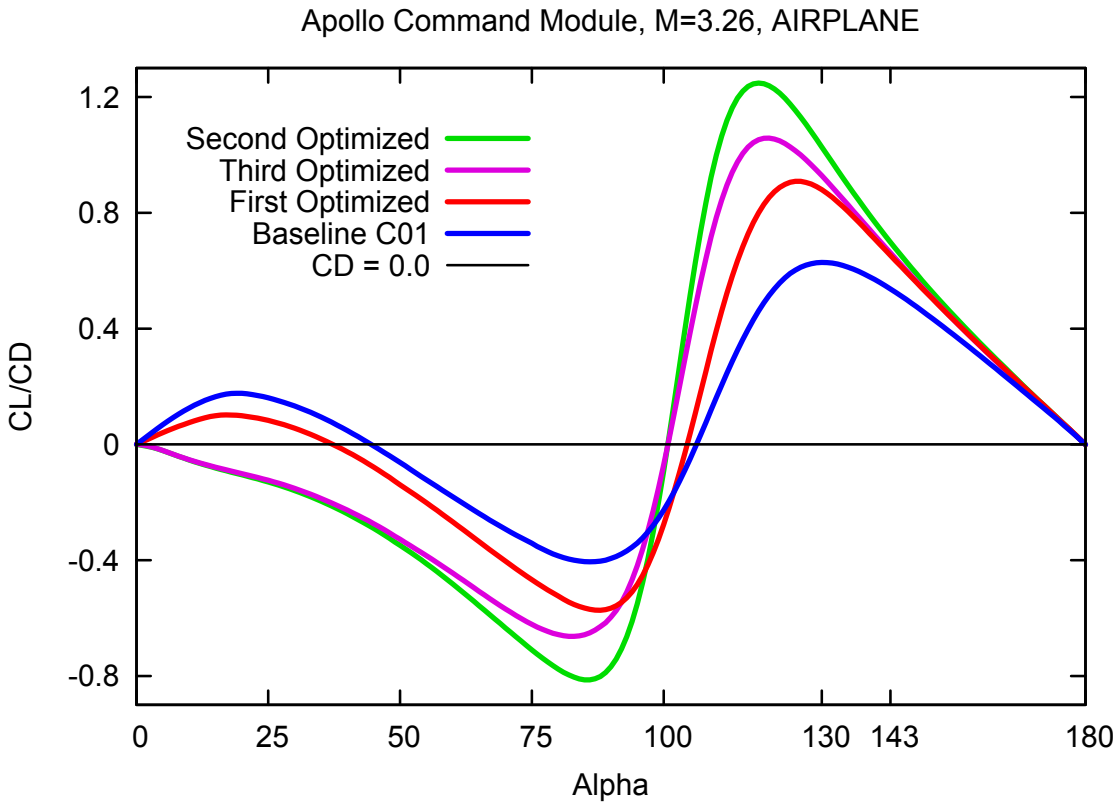

Figure 52. Alpha 0 to 180 lift-to-drag performance computed by AIRPLANE for baseline C01 and the three NPSOL optimized cases. Compare with figure 32.

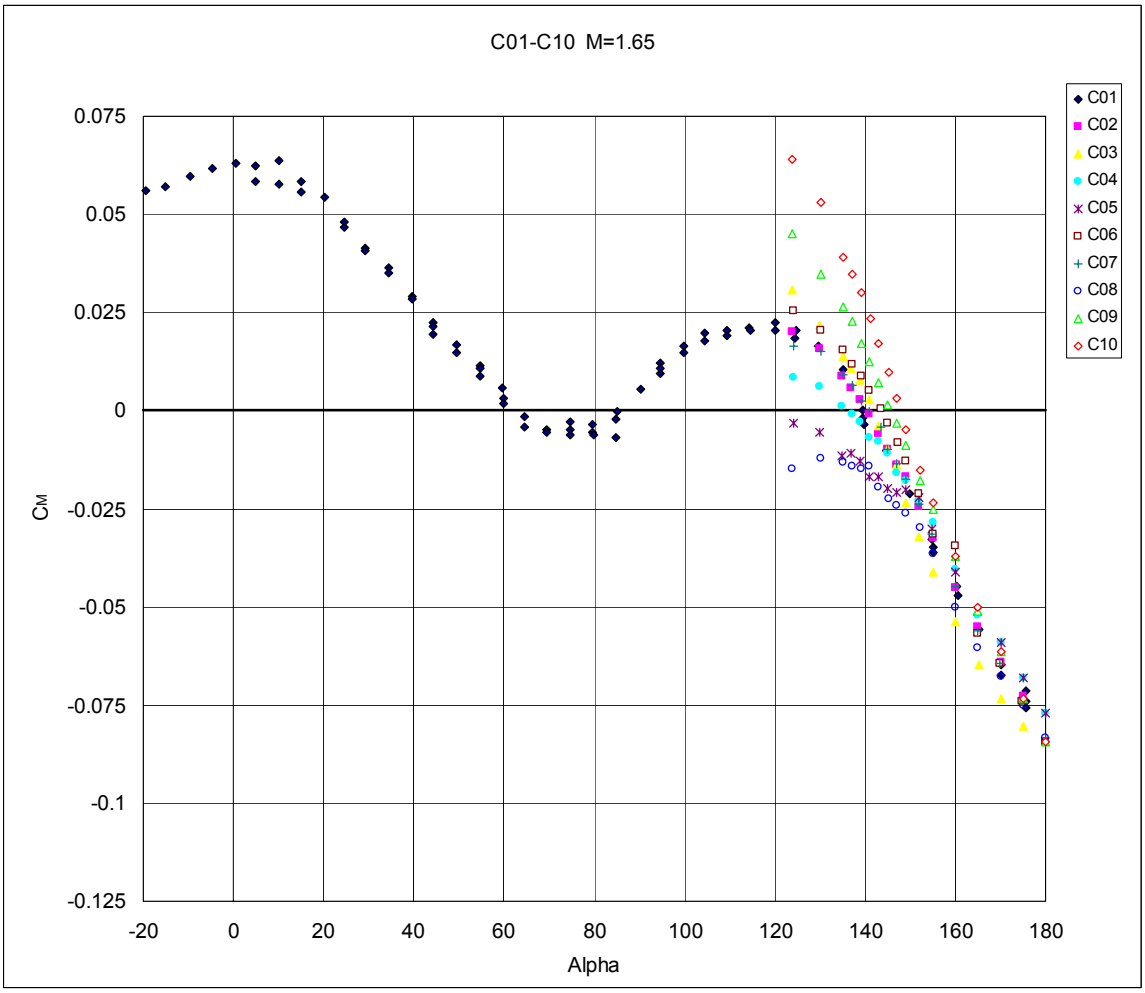

Figure 53. Wind tunnel derived pitching moment coefficient data for C01–C10 Configurations at Mach 1.65.

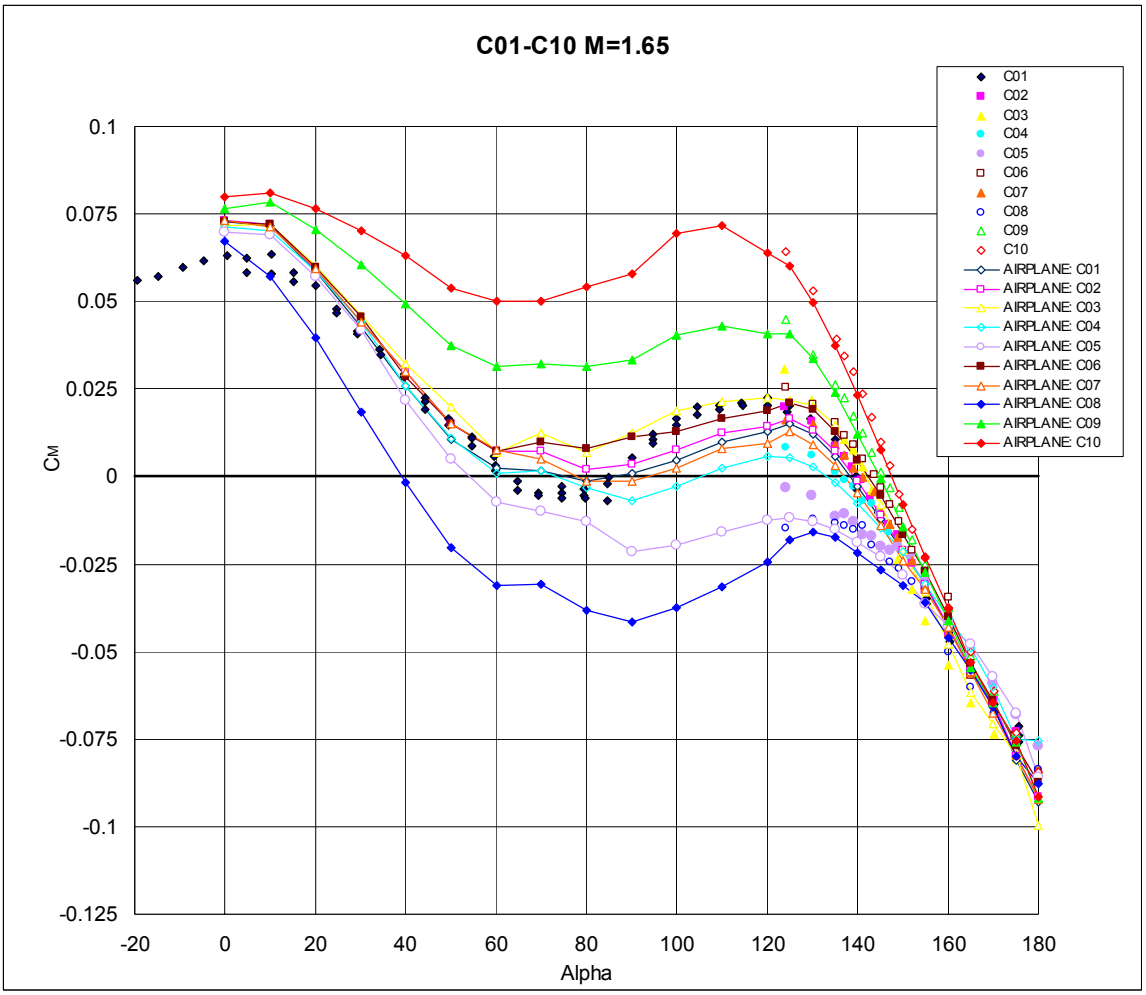

Figure 54. Computational/experimental data corroboration of pitching moment coefficient data for C01–C10 configurations at Mach 1.65, $0 \leq \alpha \leq 180$.

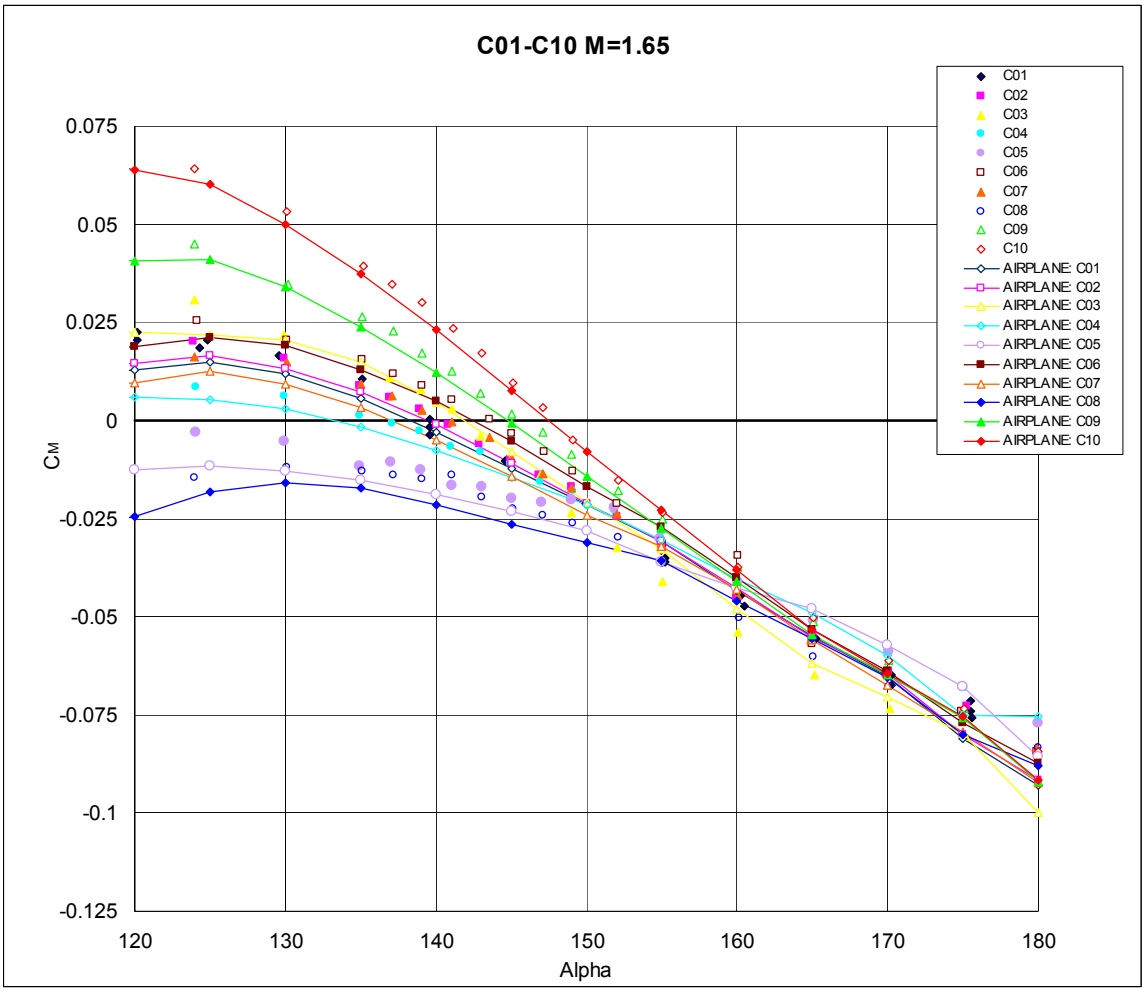

Figure 55. Computational/experimental data corroboration of pitching moment coefficient data for C01–C10 configurations at Mach 1.65, $120 \leq \alpha \leq 180$.

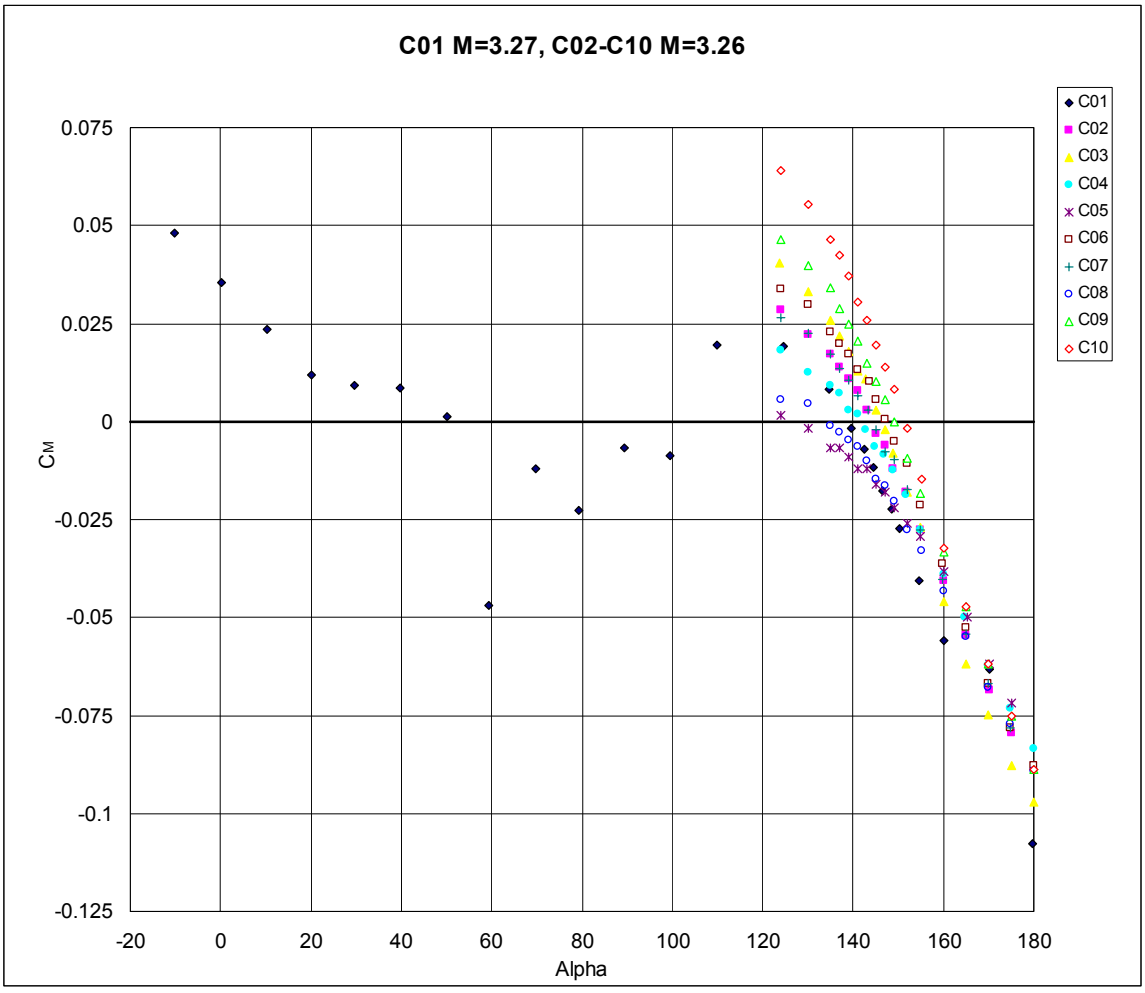

Figure 56. Wind tunnel derived pitching moment coefficient data for C01–C10 configurations at Mach 3.26 and 3.27.

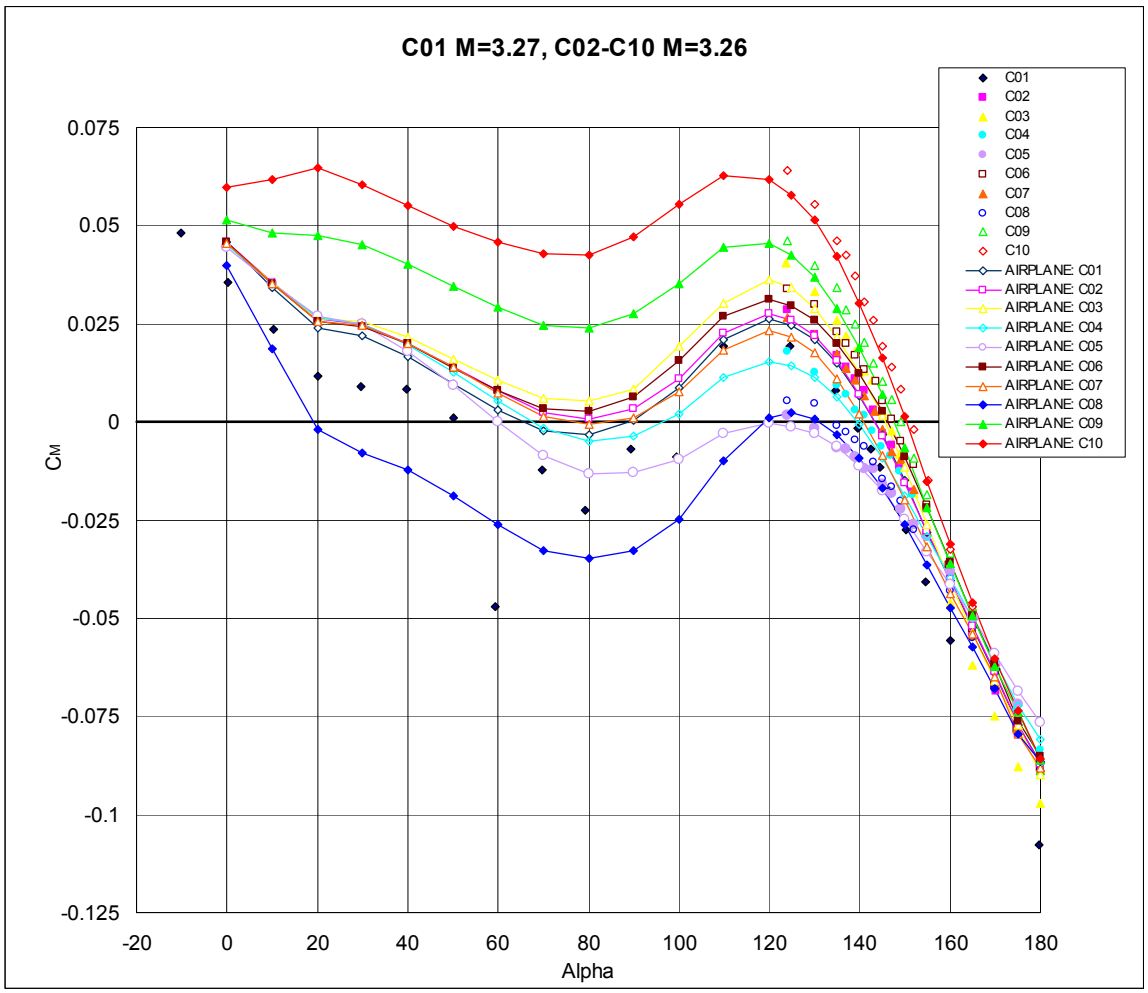

Figure 57. Computational/experimental data corroboration of pitching moment coefficient data for C01–C10 configurations at Mach 3.26 and 3.27, $0 \leq \alpha \leq 180$.

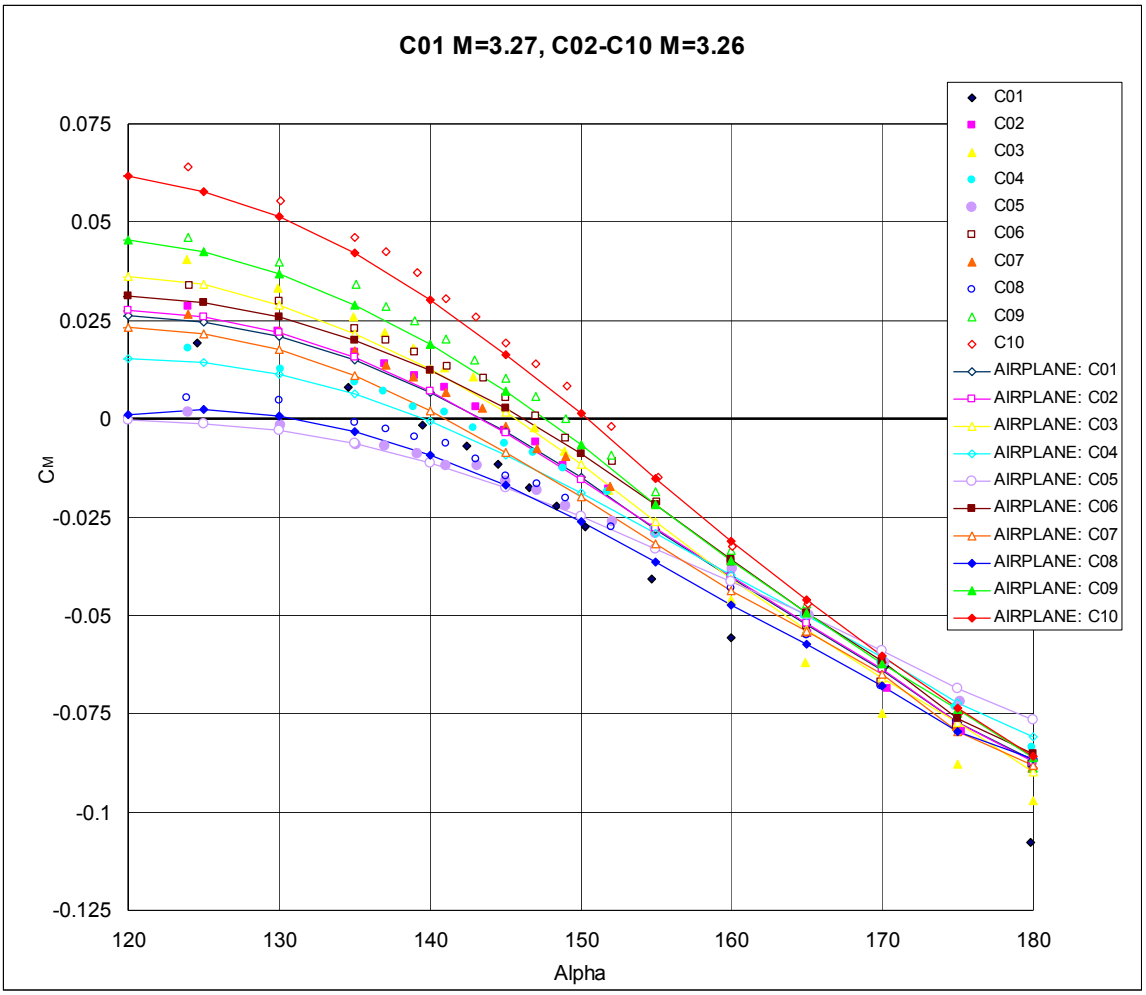

Figure 58. Computational/experimental data corroboration of pitching moment coefficient data for C01–C10 configurations at Mach 3.26 and 3.27, $120 \leq \alpha \leq 180$.

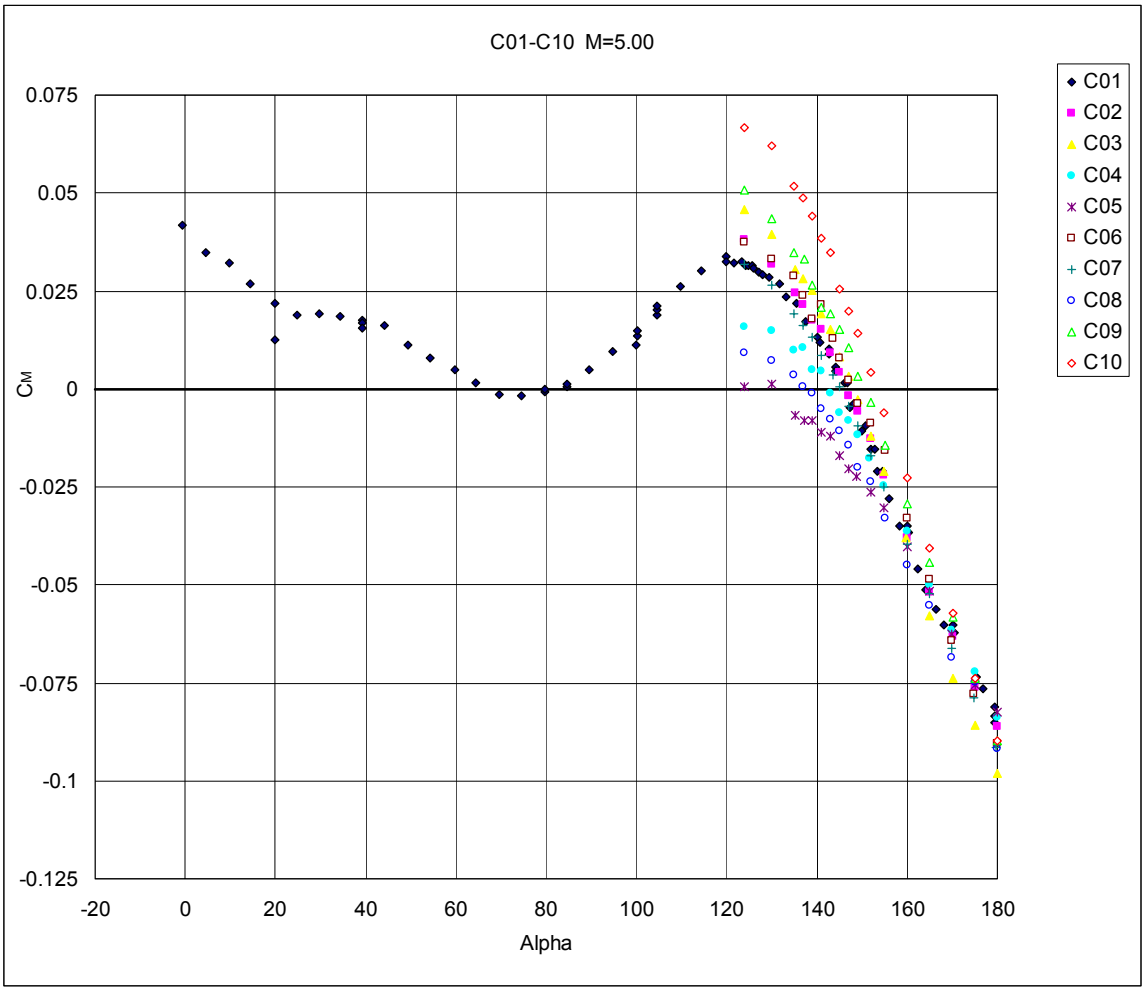

Figure 59. Wind tunnel derived pitching moment coefficient data for C01–C10 Configurations at Mach 5.0.

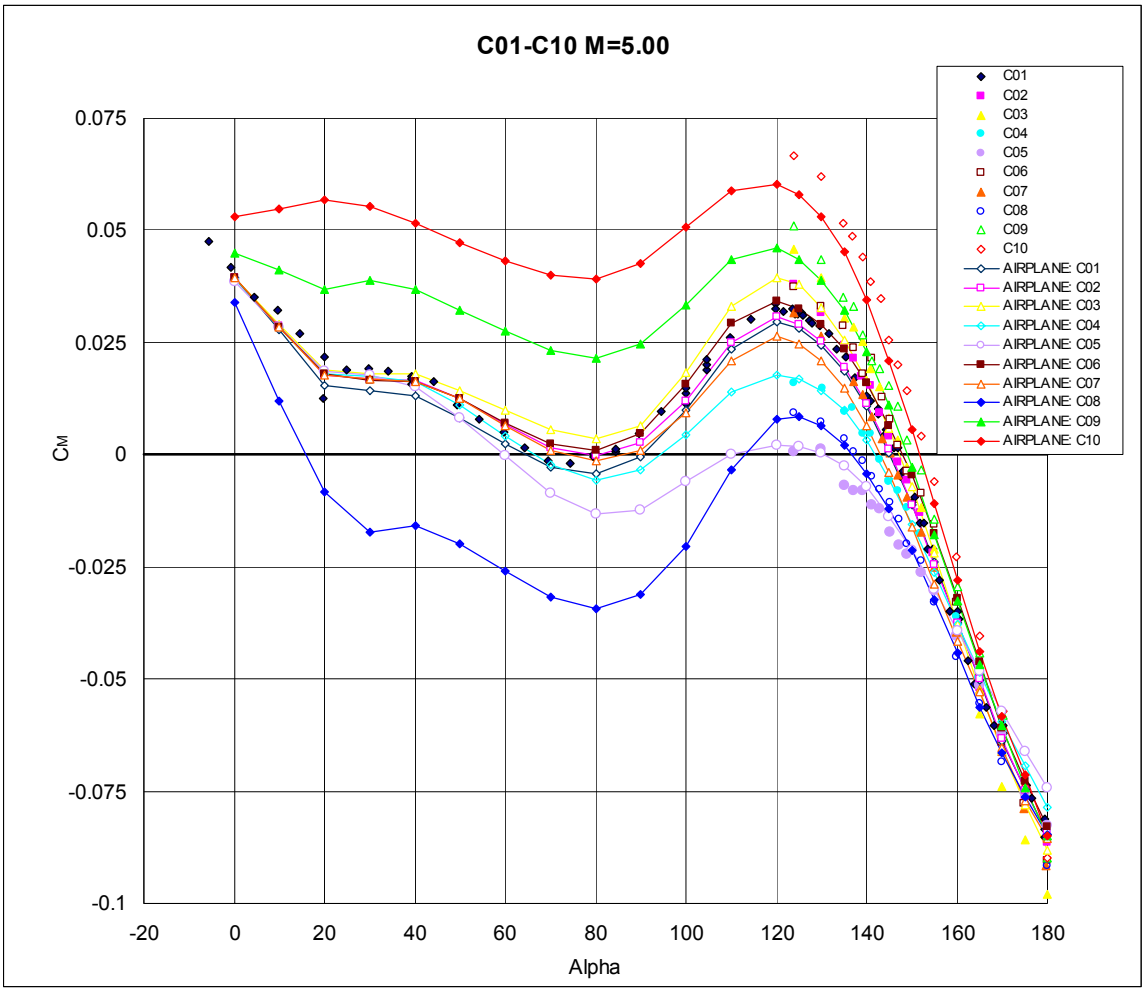

Figure 60. Computational/experimental data corroboration of pitching moment coefficient data for C01–C10 configurations at Mach 5.0, $0 \leq \alpha \leq 180$.

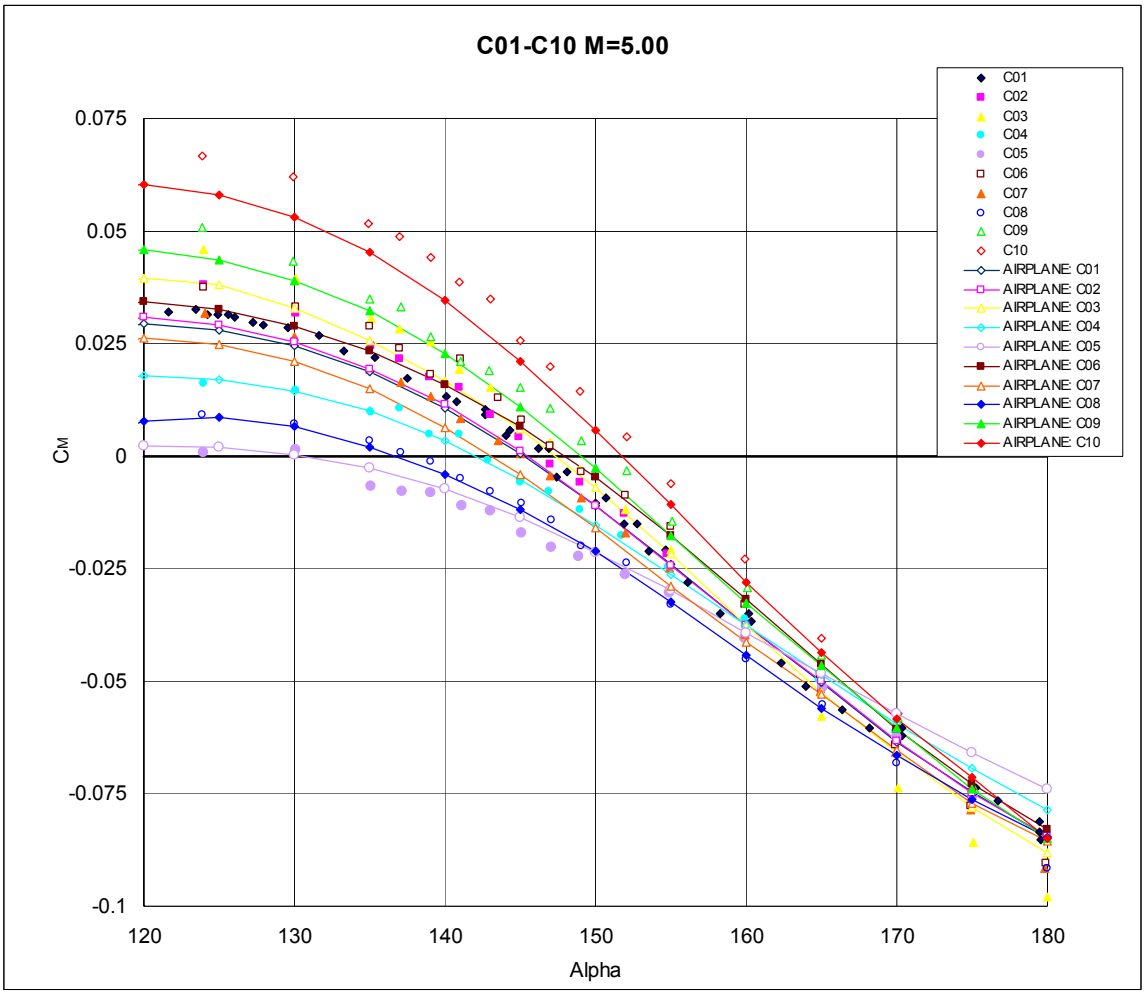

Figure 61. Computational/experimental data corroboration of pitching moment coefficient data for C01–C10 configurations at Mach 5.0, $120 \leq \alpha \leq 180$.

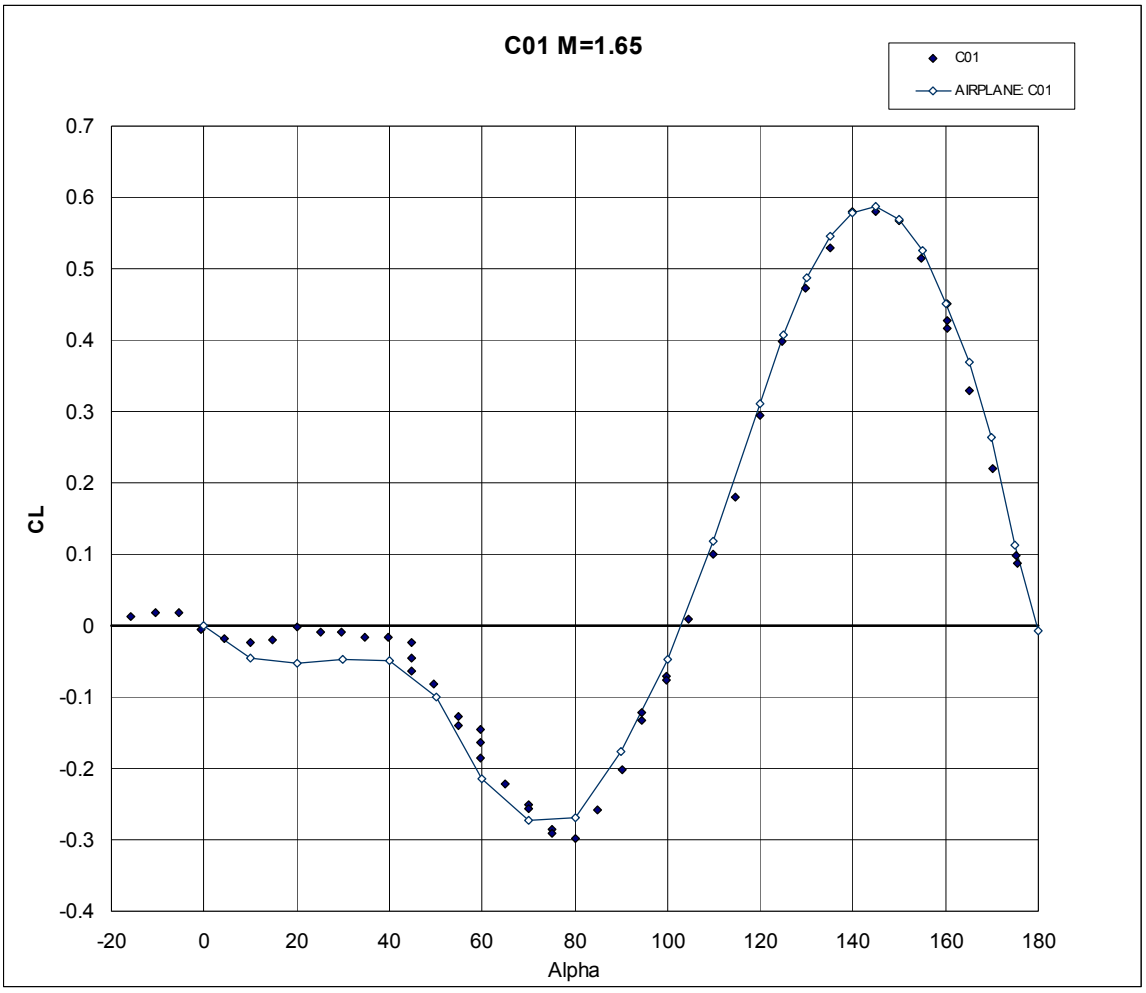

Figure 62. Lift coefficient comparison for the C01 configuration at Mach 1.65.

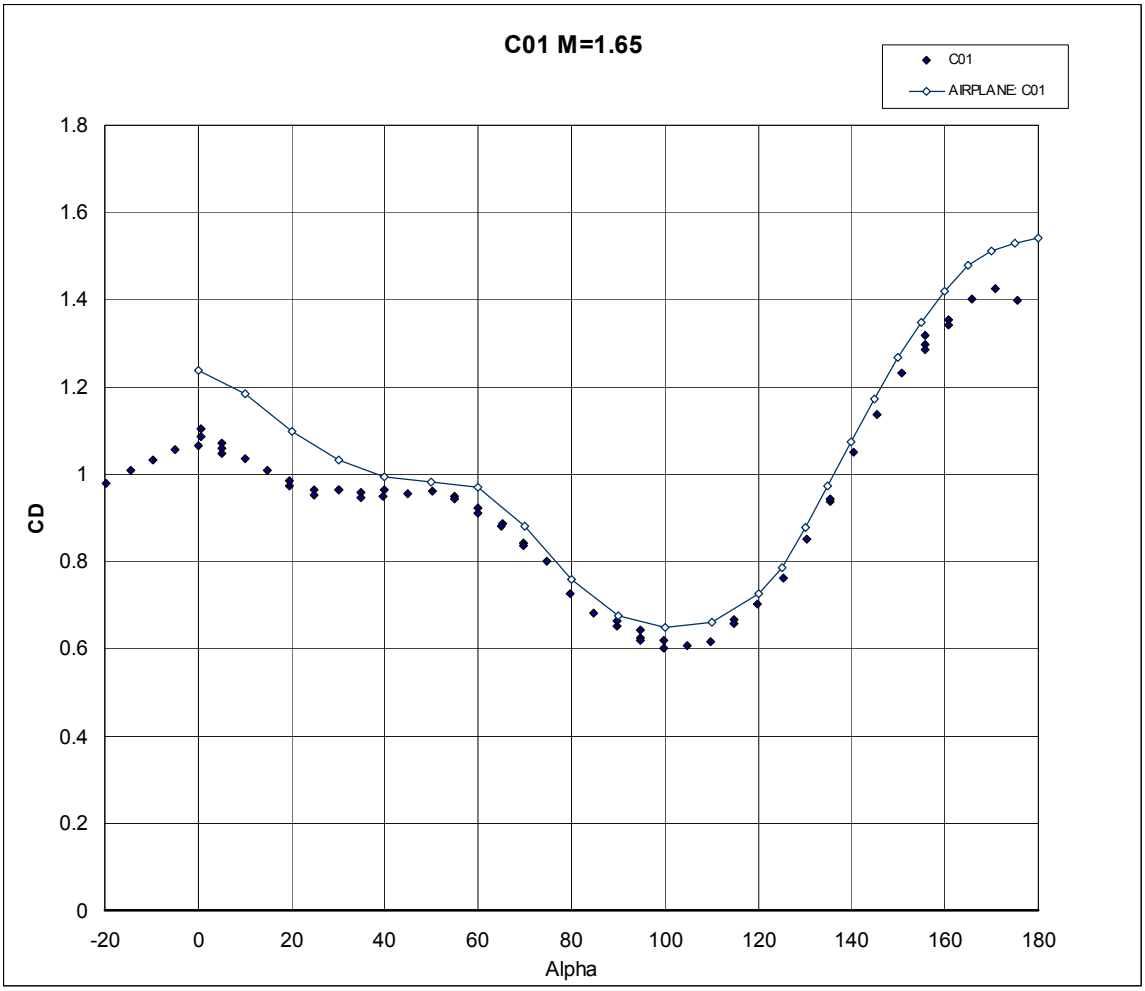

Figure 63. Drag coefficient comparisons for the C01 configuration at Mach 1.65.

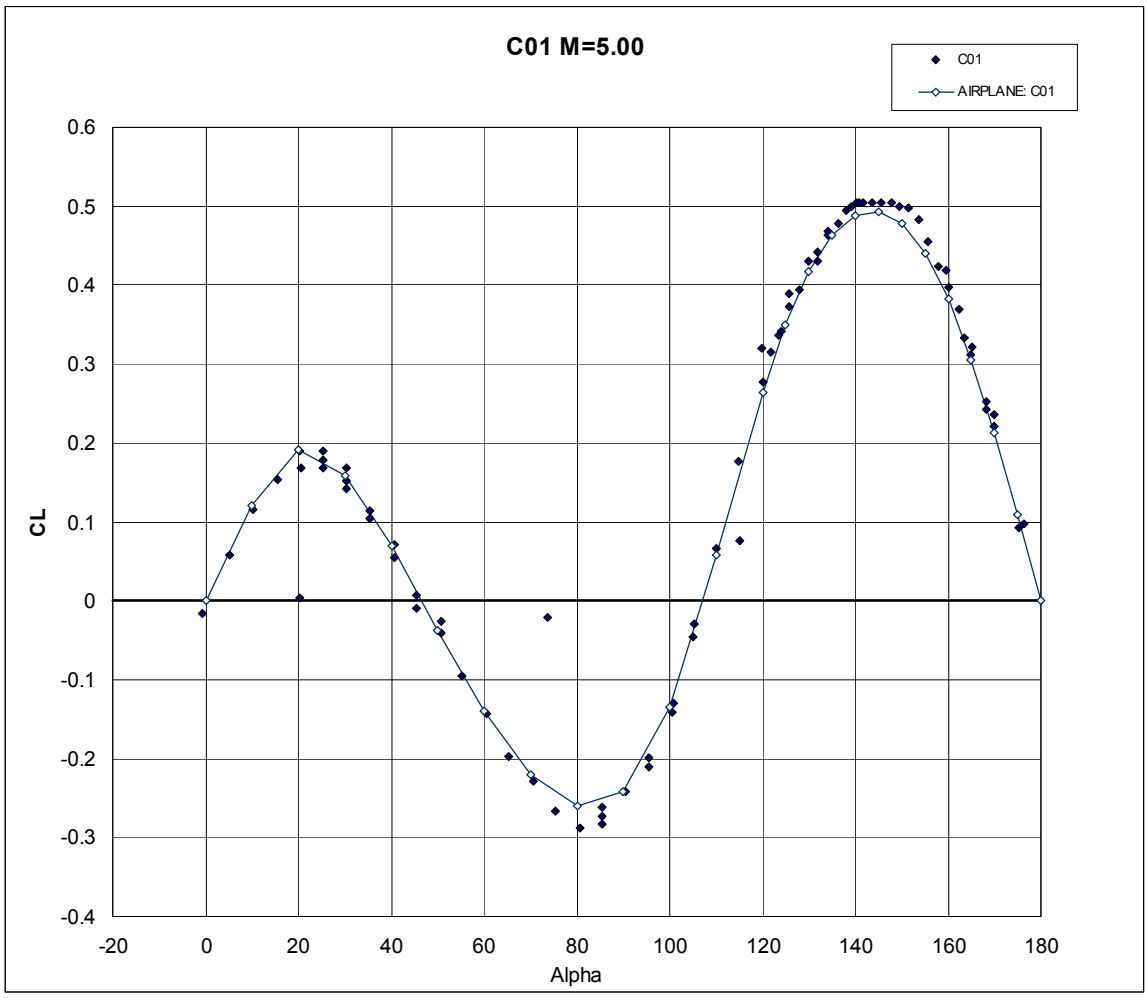

Figure 64. Lift coefficient comparisons for the C01 configuration at Mach 5.0.

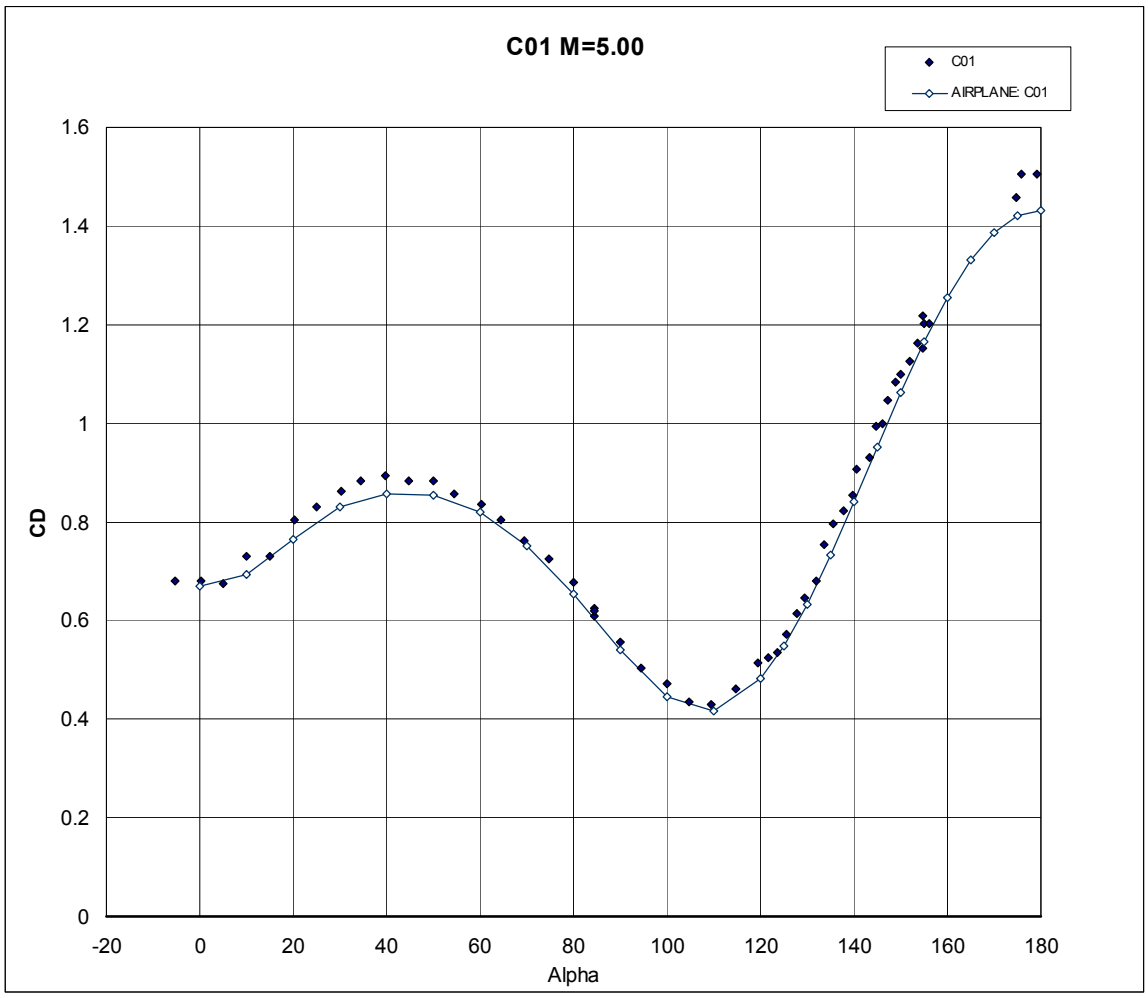

Figure 65. Drag coefficient comparisons for the C01 configuration at Mach 5.0.

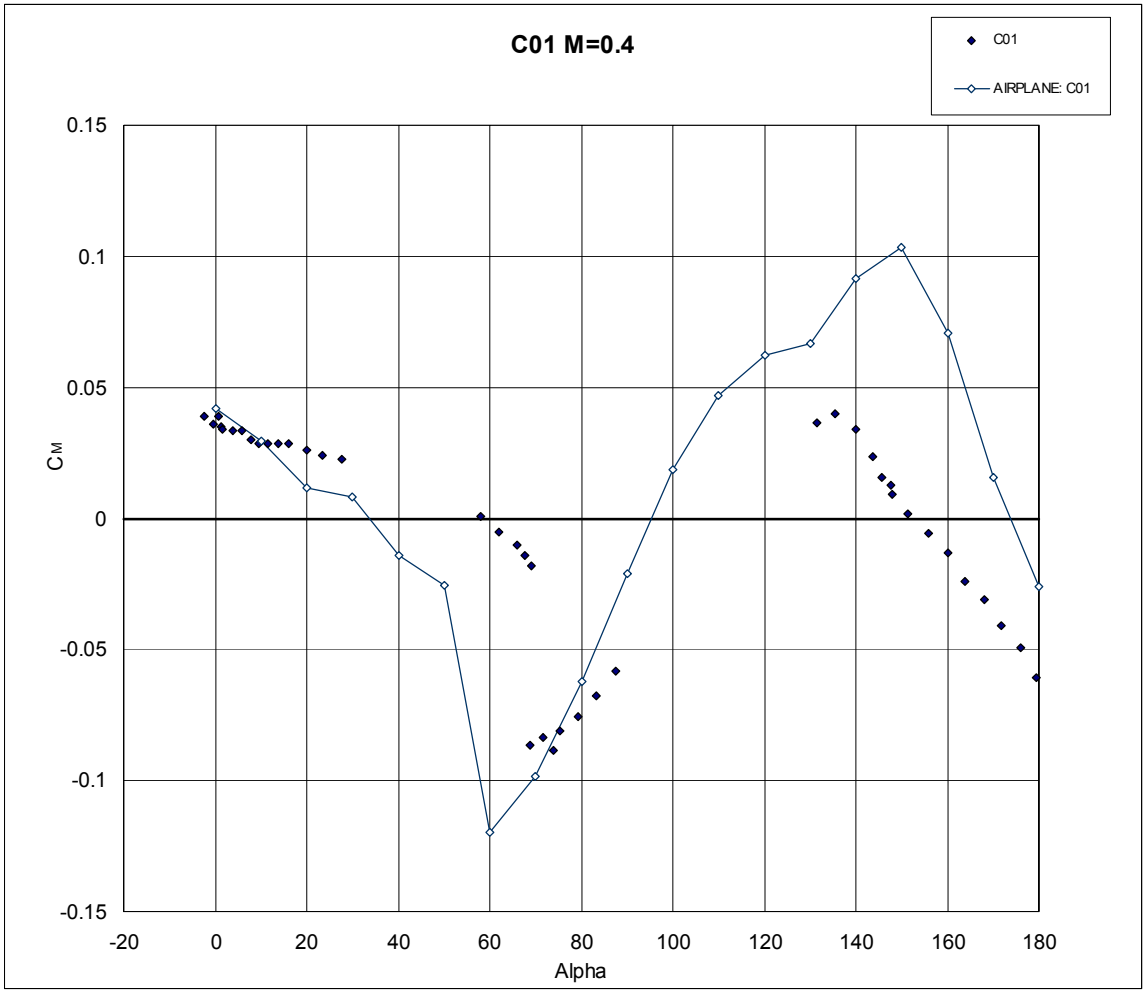

Figure 66. Pitching moment coefficient data for Mach 0.4.

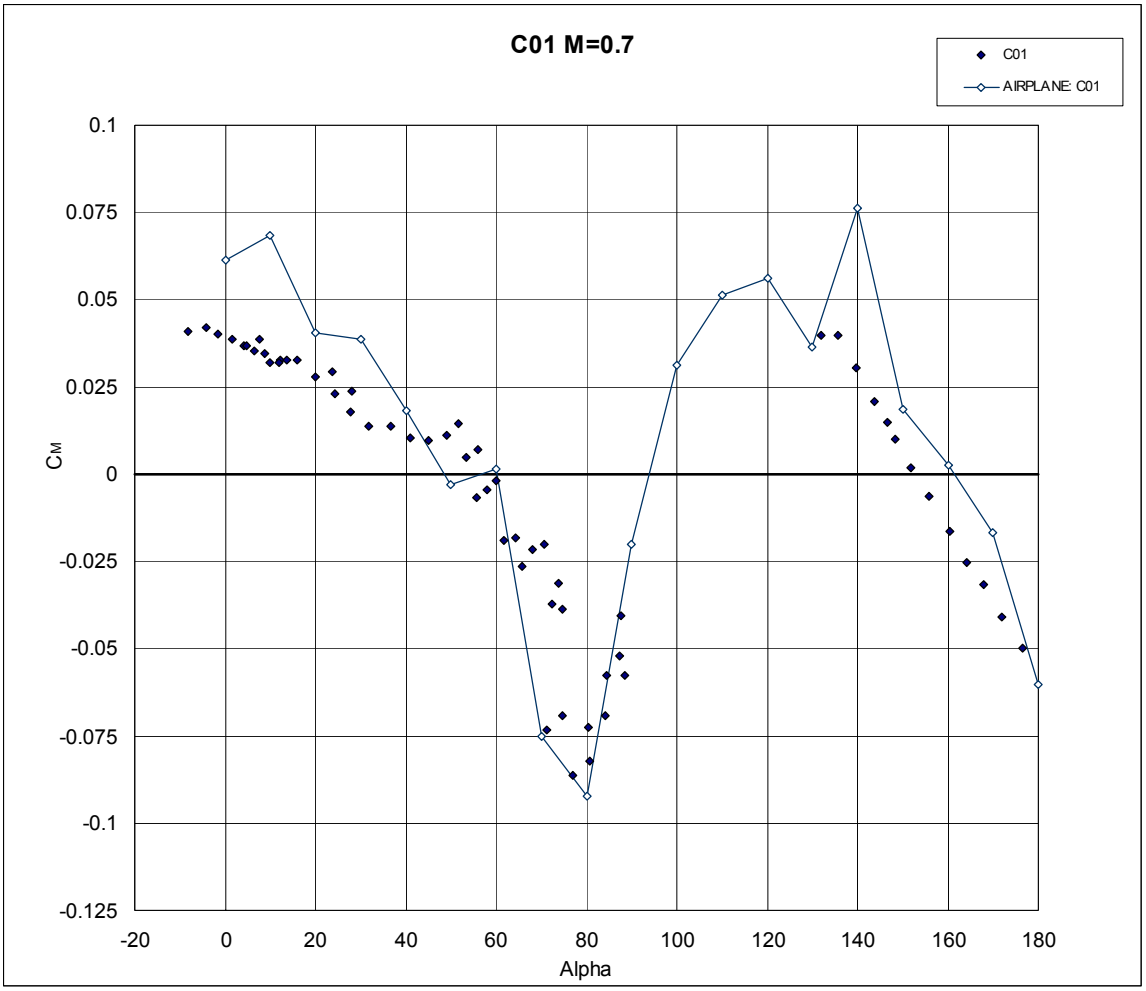

Figure 67. Pitching moment coefficient data for Mach 0.7.

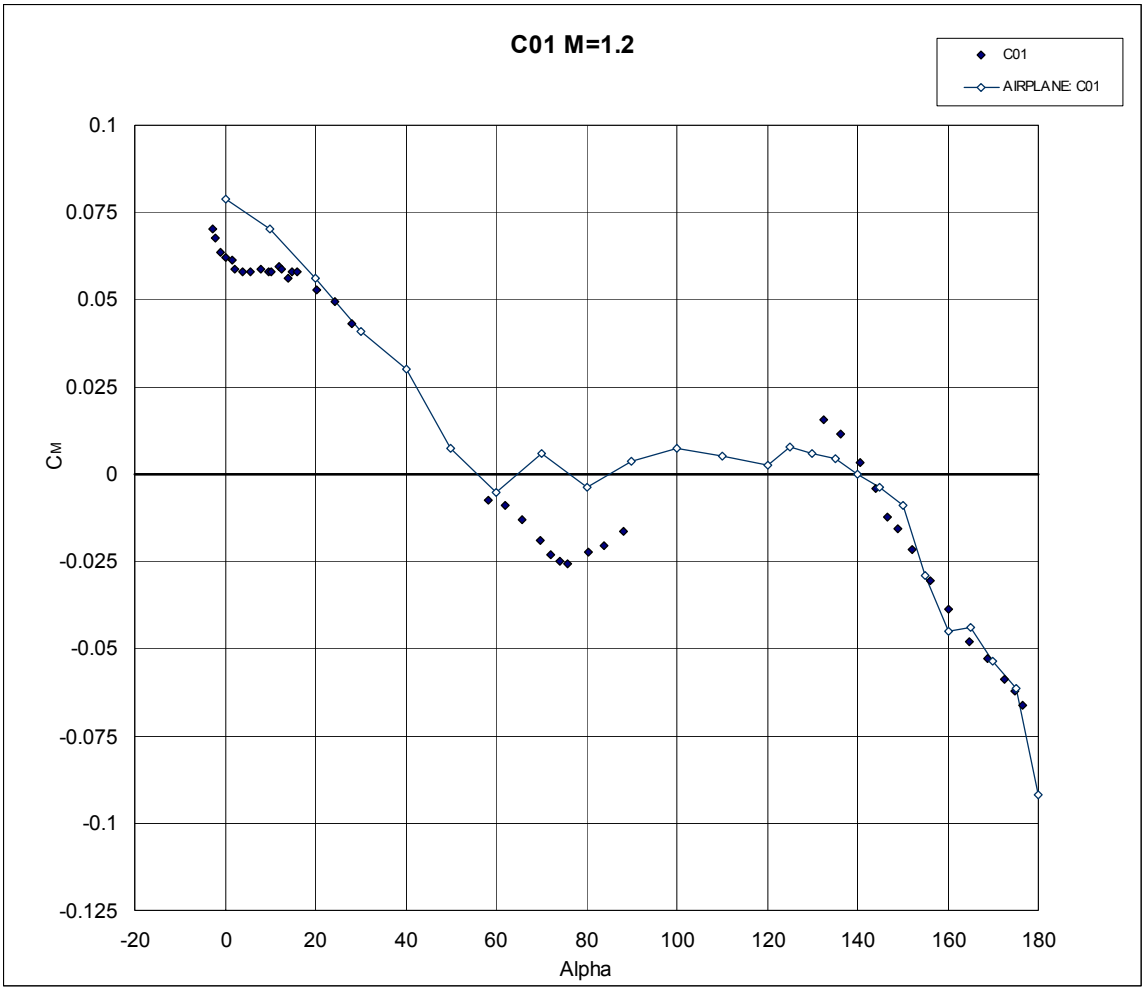

Figure 68. Pitching moment coefficient data for Mach 1.2.

REPORT DOCUMENTATION PAGE

Form Approved
OMB No. 0704-0188

1. REPORT DATE *(DD-MM-YYYY)*	2. REPORT TYPE	3. DATES COVERED *(From - To)*
05/20/2005	Technical Memorandum	

4. TITLE AND SUBTITLE

The Apollo Capsule Optimization for Improved Stability and Computational/Experimental Data Comparisons

5a. CONTRACT NUMBER

5b. GRANT NUMBER

5c. PROGRAM ELEMENT NUMBER

6. AUTHOR(S)
Susan E. Cliff and Scott D. Thomas

5d. PROJECT NUMBER

5e. TASK NUMBER

5f. WORK UNIT NUMBER
21-982-10-20

7. PERFORMING ORGANIZATION NAME(S) AND ADDRESS(ES)
Ames Research Center, Moffett Field, CA 94035-1000
and
Raytheon ITSS, Ames Research Center, Moffett Field, CA 94035-1000

8. PERFORMING ORGANIZATION REPORT NUMBER
A-0513777

9. SPONSORING/MONITORING AGENCY NAME(S) AND ADDRESS(ES)
National Aeronautics and Space Administration
Washington, D.C. 20546-0001

10. SPONSORING/MONITOR'S ACRONYM(S)
NASA

11. SPONSORING/MONITORING REPORT NUMBER
NASA/TM-2005-213457

12. DISTRIBUTION/AVAILABILITY STATEMENT
Unclassified — Unlimited Distribution: Nonstandard
Subject Category: 08, 18
Availability: NASA CASI (301) 621-0390

13. SUPPLEMENTARY NOTES
POC: Susan E. Cliff, Ames Research Center, Analysis Branch, MS 258-1, Moffett Field, CA 94035-1000
(650) 604-3907

14. ABSTRACT

Numerical optimization was employed on the Apollo Command Module to modify its external shape. The Apollo Command Module (CM) that was used on all NASA human space flights during the Apollo Space Program is stable and trimmed in an apex forward (alpha of approximately 40 to 80 degrees) position. This poses a safety risk if the CM separates from the launch tower during abort. Optimization was employed on the Apollo CM to remedy the undesirable stability characteristics of the configuration. Geometric shape changes were limited to axisymmetric modifications that altered the radius of the apex (R_A), base radius (R_O), corner radius (R_C), and the cone half angle (θ), while the maximum diameter of the CM was held constant. The results of multipoint optimization on the CM indicated that the cross-range performance can be improved while maintaining robust apex-aft stability with a single trim point. Navier-Stokes computations were performed on the baseline and optimized configurations and confirmed the Euler-based optimization results. Euler Analysis of ten alternative CM vehicles with different values of the above four parameters are compared with the published experimental results of numerous wind tunnel tests during the late 1960's. These comparisons cover a wide Mach number range and a full 180-degree pitch range and show that the Euler methods are capable of fairly accurate force and moment computations and can separate the vehicle characteristics of these ten alternative configurations.

15. SUBJECT TERMS
Optimization, Space capsules, Stability, Aerodynamic shape optimization, Euler, Experiment, Computational fluid dynamics (CFD)

16. SECURITY CLASSIFICATION OF:			17. LIMITATION OF ABSTRACT	18. NUMBER OF PAGES	19a. NAME OF RESPONSIBLE PERSON
a. REPORT	b. ABSTRACT	c. THIS PAGE			Susan E. Cliff
Unclassified	Unclassified	Unclassified	Unclassified	66	19b. TELEPHONE *(Include area code)* (650) 604-3907